

Geochemical cycling during subduction initiation: evidence from serpentinized mantle wedge peridotite in the south Andaman ophiolite suite

Abhishek Saha^{1*}, M. Santosh^{2,3}, Sohini Ganguly⁴, C.Manikyamba⁵, Jyotisankar Ray⁶, Jagadish Dutta¹

¹ National Institute of Oceanography (Council of Scientific and Industrial Research) Dona Paula, Goa 403 002, India

² School of Earth Science and Resources, China University of Geosciences, Beijing, China

³ Department of Earth Sciences, University of Adelaide, Adelaide SA 5005, Australia

⁴ Department of Earth Science, Goa University, Taleigao Plateau, Goa 403206, India

⁵ National Geophysical Research Institute (Council of Scientific and Industrial Research)
Uppal Road, Hyderabad 500 007, India

⁶ Department of Geology, University of Calcutta, 35, Ballygunge Circular Road, Kolkata 700 019, India

*Corresponding author: asaha.nio2015@gmail.com

Abstract

The ophiolite suite from south Andaman islands forms part of the Tethyan Ophiolite Belt and preserves the remnants of an ideal ophiolite sequence comprising a basal serpentinized and tectonised mantle peridotite followed by ultramafic and mafic cumulate units, basaltic dykes and spilitic pillow basalts inter-layered with arkosic wacke. Here we present new major, trace, rare earth (REE) and platinum group (PGE) element data for serpentinized and metasomatized peridotites (dunites) exposed in south Andaman representing the tectonized mantle section of the ophiolite suite. Geochemical features of the studied rocks, marked by $Al_2O_3/TiO_2 > 23$, LILE-LREE enrichment, HFSE depletion, and U-shaped chondrite-normalized REE patterns with $(La/Sm)_N > 1$ and $(Gd/Yb)_N < 1$, suggest contributions from boninitic mantle melts. These observations substantiate a subduction initiation process ensued by rapid slab roll-back with extension and seafloor spreading in an intraoceanic fore-arc regime. The boninitic composition of the serpentinized peridotites corroborate fluid and melt interaction with mantle manifested in terms of (i) hydration, metasomatism and serpentinization of depleted, MORB-type, sub-arc wedge mantle residual after repeated melt extraction; and (ii) refertilization of refractory mantle peridotite by boninitic melts derived at the initial stage of intraoceanic subduction. Serpentinized and metasomatized mantle dunites in this study record both MOR and intraoceanic arc signature collectively suggesting suprasubduction zone affinity. The elevated abundances of Pd (4.4-12.2 ppb) with high $\sum PPGE/\sum IPGE$ (2-3) and Pd/Ir (2-5.5) ratios are in accordance with extensive melt-rock interaction through percolation of boninitic melts enriched in fluid-fluxed LILE-LREE into the depleted mantle after multiple episodes of melt extraction. The high Pd contents with relatively lower Ir concentrations of the samples are analogous to characteristic PGE signatures of boninitic magmas and might have resulted by the infiltration of boninitic melts into the depleted and residual mantle wedge peridotite during fore-arc extension at the initial stage of intraoceanic subduction. The PGE patterns with high Os+Ir (2-8.6 ppb) and Ru (2.8-8.4 ppb) also suggest rejuvenated by infiltration of melts derived by high degree of mantle melting. The trace, REE and PGE data presented in our study collectively reflect heterogeneous mantle compositions and provide insights into ocean-crust-mantle interaction and associated geochemical cycling within a suprasubduction zone regime.

Keywords: South Andaman Ophiolite; Mantle peridotite; Metasomatism; Geochemical cycling; Subduction initiation

1. Introduction

Ophiolites are slivers of ancient oceanic lithosphere comprising fossil oceanic crust and upper mantle fragments that preserve comprehensive record of magmatic, tectonic and mineralization processes associated with construction and consumption of ancient ocean basins (Dilek, 2014; Coleman, 1984; Dilek and Furnes, 2011). In general, ophiolites are broadly characterized by spatially and temporally related refractory mantle lithologies, ultramafic-mafic plutonic rock assemblage associated with volcanic intrusions, sedimentary and metamorphic rock units that collectively provide insights into the various evolutionary stages in the life cycle of an ocean basin from rift-drift, sea-floor spreading to subduction initiation, final closure and incorporation onto continental margins during collisional orogenic events (Karipi et al., 2006; Pagé et al., 2009; Pearce and Robinson, 2010; Saccani et al., 2015). Geochemical studies of these obducted slabs of old oceanic lithosphere are particularly important for understanding different stages of melt generation during magmatic evolution of oceanic crust in ancient spreading centres and constraining the tectonic processes involved in the emplacement history of accreted units of arc-basin systems (Shervais, 2001; Pearce, 2003; Aldanmaz et al., 2008).

Mantle peridotites from ophiolite suites represent the upper mantle section and their detailed geochemical studies provide important information on melting processes, melt extraction episodes and interaction of oceanic crust, mantle melts and fluids in the paleo-oceanic lithosphere-asthenosphere system under active tectonic conditions (Kelemen et al., 1992; Barth et al., 2003; Dilek et al., 2007; Ishiwaka et al., 2007). Fluid/melt percolation and fluid/melt-mantle interaction are considered as dominant factors modifying the composition of sub-arc mantle, whereas the arc magmas derived by partial melting of mantle wedge preserve the geochemical imprints in response to subduction inputs into mantle, mantle wedge metasomatism and serpentinization (Parkinson and Pearce, 1998). Apart from the extensively studied abyssal peridotites from mid-oceanic ridge settings, the suprasubduction zone (SSZ) peridotites in ophiolite complexes attracted considerable attention as they include intraoceanic fore arc peridotites and those from spreading centres above subduction zones. Peridotites in the SSZ suites provide important constraints on mantle process and extent of interaction of fluids and melts with the wedge mantle during subduction initiation and fore-arc extension (Dai et al., 2011; Kapsiotis, 2013; Moghadam et al., 2014).

The Late Mesozoic to Early Cenozoic evolution of the Tethyan Ophiolite Belt is linked to the closure of the Tethyan Ocean and collision of Indian and Eurasian plates (Pal et al., 2003; Ghosh et al., 2017). These two tectonic events were marked by plate convergence, subduction of oceanic lithosphere, ophiolite obduction, high pressure-low temperature metamorphism and collision-accretion activities leading to the construction of the Alpine-Himalayan and Burmese-Indonesian arc systems

(Dilek et al., 1999; Robertson, 2002; Aldanmaz et al., 2008). The Tethyan Ophiolite Belt extends from Baltic Cordillera and rift of Spain and Africa eastwards through Alps, the Dinarides in Yugoslavia, through Greece, Turkey, Iran, Oman, Pakistan and the Himalayas, Burma, Andaman-Nicobar islands and Indonesia (Haldar, 1984; Saha et al., 2010). The Andaman-Java arc trench system in the Andaman sea/Bay of Bengal is the manifestation of active subduction of the Indian oceanic lithosphere beneath the Burmese plate spanning from the Cretaceous to the present (Bandyopadhyay, 2005; Chakraborty and Pal, 2001; Jafri et al., 1990). The ophiolite suite from south Andaman islands represents an ideal sequence comprising a basal-serpentinized and tectonised mantle peridotite followed by ultramafic and mafic cumulate units, basaltic dykes and spilitic pillow basalts interlayered with arkosic wacke. Podiform chromites and chromian spinels from mantle rocks of Andaman ophiolite have been studied to understand the petrogenesis and geodynamic setting (Ghosh et al., 2009, 2013; Ghosh and Bhatta, 2014). However, trace and platinum group element (PGE) compositions of serpentinized mantle peridotites of Andaman ophiolite have not been considered so far in understanding the geochemical cycling through ocean-crust-mantle and upper mantle evolution through melt extraction and refertilization processes. In this study, we present major, trace including rare earth element (REE) and platinum group element (PGE) compositions of serpentinized mantle peridotites from the Andaman Ophiolite Belt with a view to evaluate their petrogenesis and geodynamic implications. Our results provide insights into: (i) the subduction initiation processes in an intraoceanic setting ensued by forearc spreading (ii) metasomatism and melting of depleted mantle wedge by influx of slab-dehydrated fluid (iii) percolation of subduction-derived melts, melt-rock interaction and mantle refertilization (iii) serpentinization of peridotitic mantle by slab-dehydrated fluids and (iv) geochemical cycling during subduction initiation and ocean-crust-mantle interaction.

2. Geological setting

Cretaceous ophiolite occurrences in India have been recorded as part of the Alpine-Himalayan and Indo-Burman orogenic belts. The Andaman Ophiolite Belt (AOB) marks the southern extension of the Manipur and Burmese Arakan Yoma Belt, which is the easternmost continuation of the Tethyan Ophiolite Belt (Fig.1). The Andaman-Nicobar group of islands form an arcuate chain extending for about 850km bounded by latitude $6^{\circ} 45' N$ to $13^{\circ} 45' N$ and by longitude $92^{\circ} 15' E$ to $94^{\circ} 00' E$. These islands together with the Mentawi islands (southern extension of Andaman-Nicobar) belong to distinct structural and topographical belt that trends north-south and then curves eastward from Sumatra towards Java (Vohra et al., 1989; Sengupta et al., 1990). The Andaman, Nicobar, Nias and Mentawai islands represent the subaerial parts of the forearc ridge in the Sunda-Burmese double chain arc system and form a continuation of the Indo-Burma ranges in the north and Indonesian islands in the south.

The AOB represents the central part of the 5000 km long Burma-Java subduction complex and comprises tectono-stratigraphic units of an accretionary prism in an outer-arc setting (Pal et al., 2003; Pal, 2011). The AOB occurs in the outer arc region of the active Andaman-Java subduction system. Previous studies have recorded the occurrence of ophiolite sequences in several parts of south Andaman, including Haldar (1984), Ray et al., (1988), Shastry et al. (2001, 2002), Pal et al. (2005, 2010) (Fig.2A). According to Pal et al. (2003), this accretionary prism contains numerous north-south trending slices of Cretaceous-Palaeocene ophiolites and abundant Tertiary sedimentary rocks. However, the largest number of ophiolite slices are exposed in south Andaman, where a complete preservation of ophiolite suite extending from Port Blair ($6^{\circ} 45' N$ to $13^{\circ} 45' E$) to Chiriyatapu ($6^{\circ} 45' N$ to $13^{\circ} 45' E$) stretch of south Andaman (Fig. 2B) and thrust sequence of mantle peridotite near Badmash pahar and Chouldari (Fig.2C) have been documented (Saha et al., 2010).

3. Sampling and analytical techniques

Representative samples from mantle peridotite section of ophiolite suite were collected systematically from Badmash pahar ($11^{\circ} 39' N$: $92^{\circ} 39.6' E$) area of south Andaman (Fig.2C). Selected samples were finely powdered in an agate mortar and were analyzed for major, trace and REE compositions along with matrix matching geochemical reference materials for quality control at CSIR-National Geophysical Research Institute (NGRI), Hyderabad. Major element concentrations were determined by X-ray fluorescence spectrometry (XRF; Phillips MAGIX PRO Model 2440), on pressed pellets prepared from powdered whole-rock samples following the method of Krishna et al. (2007). Pressed pellets (40 mm diameter) were prepared by using collapsible aluminium cups (10). These cups were filled with boric acid and about 2g of the finely powdered sample was evenly sprayed and pressed under a hydraulic press at 25-ton pressure to get a pellet (Hydraulic Press, Herzog, Germany). Certified reference material UB-N was used in order to validate the results. The trace elements including rare earth elements (REE) were analyzed by employing closed digestion method. The trace and REE concentrations were determined by using closed digestion method and the analysis was done on Inductively Coupled Plasma Mass Spectrometer (ICP-MS; Perkin Elmer SCIEX ELAN DRC II) at NGRI. Certified reference materials UB-N were run as standards and ^{103}Rh was used as an internal standard for the analysis. The analytical procedure for ICP-MS are referred to Manikyamba et al. (2013).

Platinum Group Element (PGE) concentrations were estimated by using the nickel sulphide fire-assay pre-concentration method followed by Inductively Coupled Plasma Mass Spectrometry (ICP-MS; Perkin Elmer Ellan DRC II) for PGE analysis at NGRI, Hyderabad. The analytical procedures described in Balaram et al. (2006) were adopted for determining the PGE concentrations

of the studied samples. WMG-1 and WPR-1 were used as international reference materials for PGE analyses (Balaram, 2008). The precision and accuracy obtained for the standards for major, trace, REE and PGE analyses are given in Table S1. Major, trace, REE and PGE concentrations of the mantle peridotites from south Andaman ophiolite suite are given in Table 1.

4. Petrology

Mantle peridotite forms the basal portion of the investigated South Andaman ophiolite suite as exposed in the Badmash pahar area (Figs. 2C and 3A). This unit is highly serpentinized and it represents the mantle tectonite portion. Olivine represents the dominant mineral composition and most of the olivine grains are serpentinized and forms a mesh like texture (Fig. 3B). Serpentine formed as a secondary mineral after olivine and shows a prominent enrichment in magnesium and iron in relation to that of primary olivine. Opaque minerals occur along the grain boundaries and also as secondary veins (Fig. 3C). Electron microprobe analysis of representative primary olivine grains in a previous study by Saha et al. (2010) shows Fo content in the range of 80.1 to 86.2 (Saha et al., 2010) reflecting a restitic nature of mantle peridotite. In terms of variations of CaO (wt. %) and Mn (apfu) with respect to Fo content, the olivine compositions depict a distinct seclusion from the Iherzolite field of Group I peridotite (Saha et al., 2010).

5. Geochemistry

5.1 Major elements

The mantle peridotites from South Andaman ophiolite suite show low and restricted contents of SiO₂ (40.4-42.1 wt. %), with low abundance of Al₂O₃ (0.55-0.95 wt. %), TiO₂ (0.01-0.02 wt. %), CaO (0.03-0.17 wt. %), MnO (0.1-0.2 wt. %), Na₂O (0.01-0.1 wt. %), and K₂O (0.01-0.03 wt. %), P₂O₅ (0.2 wt. %), moderate Fe₂O₃ (8.43-12.1 wt. %) and elevated MgO (34.33-37.73 wt. %). The Mg# ranging from 0.72 to 0.81 implies a primitive, less differentiated character of these ultramafic rocks. Relatively higher loss-on-ignition values (Table 1) for the studied samples suggest possible sea-floor alteration and serpentinization by hydrothermal fluids. The CIPW normative compositions of these mantle peridotites (Table S2) show an olivine normative character and are marked by the dominant presence of hypersthene. In the ACM (Al₂O₃-CaO-MgO) diagram (after Coleman, 1977) (Fig. 4A), the plots fall in the field of mantle peridotites and are comparable with the harzburgites from Izu-Bonin-Mariana fore arc. The mantle peridotite Samples are marked by typically high Al₂O₃/TiO₂ ratios ranging from 33-100 and low CaO/Al₂O₃ varying between 0.01 and 0.15 which collectively attest to their boninitic affinity. The boninitic peridotites are characterized by distinctively low Si-high Mg compositions as also reported by Umino et al. (2015) from Ogasawara (Bonin) Archipelago, Japan.

Further, the low $\text{CaO}/\text{Al}_2\text{O}_3$ (<0.75) classify these samples as low Ca-boninites reflecting relatively more depleted source than their high-Ca counterparts (Crawford et al., 1989).

5.2 Trace elements (including REE)

The studied mantle peridotites possess markedly high concentrations of Ni (2068-3432 ppm) and Cr (1067-2972 ppm) with 91-126 ppm Co. The Ni and Cr concentrations are higher than the primitive mantle values (Ni: >400 and Cr: >800 ppm). The major, trace and REE compositions conform to the distinct boninitic signatures for the studied mantle peridotites showing characteristically high $\text{Al}_2\text{O}_3/\text{TiO}_2$ ratios at $(\text{La}/\text{Sm})_{\text{N}} > 1$ and $(\text{Gd}/\text{Yb})_{\text{N}} < 2$ (Table 1). The low Ti and V contents for these rocks are analogous to dunites and harzbugites from Izu-Bonin-Mariana fore arc and substantiate their boninitic affinity. (Fig. 4B). Chondrite normalized REE patterns for the studied samples (Fig. 5) reflect pronounced LREE/MREE fractionations with $(\text{La}/\text{Sm})_{\text{N}} = 2.84-5.2$ and $(\text{Gd}/\text{Yb})_{\text{N}} = 0.55-1.53$ representing depleted MREE/HREE trends thereby corroborating MREE depletion and relative LREE-HREE enrichment. Primitive mantle normalized multi-element abundance of the mantle peridotites display negative anomalies at Nb, Ta, Zr, Hf, P and Ti with positive anomalies at Nd and relative enrichment in La (Fig.5). Therefore, the overall trace element chemistry of these rocks is characterized by LILE-LREE enrichment with relatively depleted HFSE concentrations.

5.3 Platinum Group Elements

The mantle peridotites samples show low (<100 ppb) total PGE contents with ΣPGE varying between 11.6-41.2 ppb. These rocks are characterized by higher concentrations of Palladium Group PGE (PPGE) than Iridium Group PGE (IPGE) marked by $\Sigma\text{PPGE}/\Sigma\text{IPGE}$ ratios in the range of 2-3 and Pd/Ir ranging from 2-5.5. The studied samples exhibit coherent chondrite normalized PGE patterns (Fig.6) with prominent enrichment of Ni, Cu, Y, Pd, Ru and relative depletion of Ir, Pt and Rh.

6. Discussion

6.1 Tectonic Implications

Based on different tectonic and petrological parameters including spreading rate and thickness of oceanic crust, proximity to plumes and trenches, fertility and temperature of mantle, as well as circulation of fluids through upper mantle lithologies, ophiolites have been classified as subduction-related and subduction-unrelated types (Dilek, 2014). Subduction-related ophiolites include suprasubduction zone (SSZ) and volcanic arc (VA) ophiolites that preserve subduction signatures and are associated with the closure of ocean basins. Subduction-unrelated ophiolites such as continental-margin, plume-proximal, plume-distal and trench-distal mid-oceanic ridge and plume-type ophiolites

develop under rift-drift conditions during sea-floor spreading and are geochemically characterized by MORB compositions (Dilek, 2003; Dilek et al., 2007; 2008; Dilek and Furnes, 2009). Further, the concept of suprasubduction zone (SSZ) ophiolites brought up a new paradigm envisaging paleo-oceanic lithosphere evolution. Studies on SSZ ophiolites particularly addressed diagnostic geochemical signatures of ophiolite suites that are suggestive of multiple episodes of mantle melting and changing tectonic scenario linked to initial stages of subduction and associated sea-floor spreading in fore-arc region (Santosh et al., 2013; Yang et al., 2016). Therefore, mantle sections of SSZ ophiolites differ from abyssal peridotites of 'MORB' ophiolites in their association with fore-arc extension above subducted oceanic lithosphere and evolution through magmatic and tectonic processes of intraoceanic subduction environments (Shervais, 2001; Ishikawa et al., 2002; Moghadam et al., 2014; Xiong et al., 2017).

Th and Nb serve as useful proxies for interpreting geochemical and tectonic affinities of a wide variety of basaltic magmas generated in divergent, convergent and intra plate environments (Saccani, 2015). Discrimination figures (Figs. 7A and 7B) based on Th and Nb systematics distinguish three different types of convergent plate margin settings (Figs. 7A and 7B) demarcating distinct fields for island arcs with (i) complex polygenetic crustal signatures (ii) increasing Th/Nb indicating interaction between subduction components and mantle wedge and (iii) decreasing Th/Nb compositions defining an array of mantle depletion without input from subduction derived components. Back-arc basin basalts have been distinguished into immature and mature intraoceanic back-arcs separated by fields marked by variable contribution from subduction/crustal components (Back arc 'A') and no contribution from subduction/crustal materials (Back arc 'B'). In $(Th)_N$ vs. $(Nb)_N$ tectonic discrimination plot (Fig. 7A) all the mantle peridotite samples in this study correspond to the volcanic arc array thereby showing affinity towards subduction zone settings associated with intraoceanic convergent plate margins. The plots for the studied samples fall close to the field for island arc tholeiites and boninites implying increasing contributions from subduction components. Further, the sample array for the mantle peridotites of south Andaman Ophiolite suite reflects forearc and intra-arc oceanic subduction-related environment (Fig. 7B) with SSZ signature. The V vs. Ti relations further reveal a boninitic affinity (Fig. 4B). Chondrite-normalized REE patterns for these rocks with MREE depletion and relative LREE-HREE enrichment are comparable with that of boninites and boninitic peridotites from South Sandwich fore arc, Dazhuka and Bainang ophiolites from Yarlung Tsangpo suture zone, Tibet (Fig. 7C). In the Al_2O_3 vs. CaO diagram (Fig. 8A), the studied mantle peridotite samples cluster within the field of forearc peridotites, while Mg/Si vs. Al/Si relations show their geochemical and tectonic compatibility with peridotites from Mariana forearc (Fig. 8B). These

geochemical attributes suggest that the studied samples bear a strong boninitic signature derived from subduction initiation processes in a typical island arc environment. These mantle peridotites with low Al_2O_3 contents correspond to the compositional range for intraoceanic fore arc peridotites and serpentinites (Fig. 8C). The overall tectonic and geochemical fingerprints of the mantle peridotites from south Andaman ophiolite suite suggest hydration, serpentinization and metasomatism of refractory mantle by slab-dehydrated fluids under extending upper plates of a fore arc subduction zone and refertilization of peridotitic mantle by boninitic melts derived during initial stages of intraoceanic subduction, typical of SSZ setting. The subduction-modified, arc-like character of the mantle peridotites with a boninitic trend particularly provides evidence for subduction initiation and serves as a key to link Andaman ophiolites with intraoceanic subduction and fore arc extension in a SSZ environment (Whattam and Stern, 2011). The genesis of Late Jurassic (~165 Ma) and Late Cretaceous (~90 Ma) ophiolites in the Eastern Mediterranean–Persian Gulf region is often related to initial stages of oceanic subduction (Stern, 2004; Pearce and Robinson, 2010; Moghadem et al. 2010). Arc-like to MORB-like geochemical imprints for Izu-Bonin-Mariana forearc and Tethyan ophiolites suggest that ophiolite complexes attest to diverse compressional and extensional tectonic processes operative during juvenile to matured stages of intraoceanic subduction and ocean floor spreading.

6.2 Geochemical characterization of serpentinized mantle peridotites and protolith signature

The geochemical composition of serpentinized peridotites is governed by various factors including: (i) temperature and nature of hydrating fluids and (ii) geodynamic setting in which they are formed. Based on the geochemical signatures and tectonic affinity, three types of serpentinized peridotites viz. abyssal, mantle wedge, and subducted have been distinguished (Deschamps et al., 2013). Abyssal serpentinites represent hydration of oceanic peridotites by seafloor hydrothermal activity and seawater alteration. Mantle wedge serpentinites are mantle peridotites hydrated by fluid released from the subducted slabs. Subducted serpentinites are more heterogeneous in terms of timing of serpentinization and are found mostly in suture zones and associated with HP–LT metamorphic rocks. They originate either from abyssal peridotites hydrated at ridges, trenches or within the subduction channel and also from the ocean–continent transition zone (OCT). Their boninitic geochemical signatures attest to their linkage with initiation of oceanic plate subduction at convergent margin settings and their SSZ affinity. In ancient and modern subduction systems, the two principle contributors to convergent margin magmatism are the mantle wedge and the subducting oceanic lithosphere (Tatsumi, 2005; Kimura and Yoshida, 2006; Dilek et al., 2008; Iwamori and Nakamura, 2015; Santosh et al., 2015; Yang and Santosh, 2017). The complex geochemical characteristics and dynamics of the mantle wedge are controlled by (i) continuous input from subducted slab in terms of

percolation by fluids released from the dehydration of subducted lithologies such as sediments, altered basalts and gabbros causing metasomatism and serpentinization, (ii) partial melting and melt extraction for arc magmas (Stern, 2002; Deschamps et al., 2011) and (iii) presence of fluids and magmas resulting from the slab dehydration that reduce the viscosity of the mantle and influence the geodynamics of the mantle wedge (Korenaga and Karato, 2008; Kelemen et al., 2003; Currie et al., 2004). Water released from the dehydrated subducted slab migrates upward by buoyancy, induce the hydration of the mantle wedge, and in particular cause serpentinization (DeShon and Schwartz, 2004; Guillot et al., 2000; Hattori and Guillot, 2003; Deschamps et al., 2013). The boninitic geochemical signatures of mantle peridotites from south Andaman ophiolite suite attest to their linkage with initiation of oceanic plate subduction at convergent margin settings and SSZ affinity. These serpentinized mantle peridotites are thus associated with a sub arc mantle wedge in an intraoceanic subduction zone and thus characterized as mantle wedge serpentinites.

The samples in this study are analogous to forearc peridotites and reflect distinct signatures of serpentinization with melt depletion trend and increasing partial melting compared to mid-oceanic ridge (MOR) peridotites (Fig. 8A). These features suggest a chemically depleted mantle modified by contributions from melts of high degree partial melting and serpentinization within an intraoceanic fore arc. Petrographic characters and geochemical attributes suggest that these mantle wedge serpentinites are mainly derived from dunite in a highly refractory mantle that witnessed extensive partial melting and melt extraction (Fig. 9A). Preservation of the refractory signature of their protoliths (Deschamps et al., 2010; Marchesi et al., 2009), and geochemical evidence of mantle wedge metasomatism by melts and/or fluids prior to serpentinization (Deschamps et al., 2010; Parkinson and Pearce, 1998; Savov et al., 2005; 2007) provide reliable clues for geochemical characterization and identification of protoliths of the serpentinized mantle wedge dunites. The geochemistry of mantle rocks have been employed to assess increasing degrees of melt extraction, from passive margins to mature oceans to subduction zones (Bonatti and Michael, 1989). Moreover, numerous processes like fluid-rock and/or melt/rock interactions prior to serpentinization could also modify the compositions of peridotites, within the mantle wedge (Pearce et al., 2000). The REE chemistry of serpentinites can be used to decipher the nature of the protolith and the interactions with fluid/melt. The $(LREE)_{CN}$ contents of the studied samples are comparable to serpentinites formed from mantle wedge dunites, with a range of ~ 0.005 to ~ 0.1 ppm and $(HREE)_{CN}$ from ~ 0.02 to ~ 0.2 ppm and serpentinites after harzburgites with $(LREE)_{CN}$ content varying from ~ 0.001 to ~ 0.2 ppm and $(HREE)_{CN}$ from ~ 0.02 to ~ 0.5 ppm. The U-shaped REE patterns marked by relative LREE and HREE enrichments and MREE depletion [$(La/Sm)_N = 2.84-5.2$ and $(Gd/Yb)_N = 0.55-1.53$], and the negative Eu anomalies displayed

by these rocks are geochemically analogous to serpentized mantle wedge serpentized dunites. Their Mg, Al and Si contents are analogous to those of the Mariana forearc peridotites (Fig.8B). The LREE enriched signatures of the serpentized mantle dunites are interpreted as the result of the combination of extensive partial melting and subsequent percolation of LREE-rich fluids or melts through the mantle wedge, whereas their HREE compositions are similar to those observed in ultramafic rocks that experienced high degree of melt extraction (Bodinier and Godard, 2003). The distinct U-shaped REE patterns for the studied samples suggest a multi-stage petrogenetic process for mantle wedge dunite protolith that experienced extensive melt extraction (Fig.9A) rendering a depleted mantle residue and fertilization of the refractory mantle residue by infiltration of melts of boninitic compositions. The boninitic melts were derived by fluid-fluxed metasomatism of mantle wedge during initial stage of subduction followed by hydrous melting at shallow depth. The characteristic U-shaped REE patterns for serpentized mantle wedge peridotites of south Andaman ophiolite suite are comparable with those of the Zhangbo ophiolite from Yarlung-Zhangbo suture zone (Dai et al., 2011), the Antalya and the Ortaca ophiolite in southwestern Turkey (Uysal et al., 2007; Aldanmaz et al., 2009; Caran et al., 2010), the Sapat peridotite in Kohistan, northwestern Pakistan (Bouilhol et al., 2009), the Othris and the Kallidromon ophiolite in Greece (Karipi et al., 2006; Barth et al., 2008), the Khoy ophiolite in northwestern Iran (Monsef et al., 2010), the Yushigou ophiolites in the North Qilian (Song et al., 2009), the Wutaishan peridotites in North China (Polat et al., 2006), and the Luobusa, Zedang and the Xigaze ophiolite in southern Tibet (Bédard et al., 2009; Bezard et al., 2011; Li et al., 2015).

Primitive mantle normalized trace element patterns for the studied samples (Fig.5) show distinct depletion in HFSE with relative LILE and LREE enrichment. The HFSE depletion in the samples is interpreted in terms of high degrees of melt extraction, however, retention of fluid immobile HFSE can also result in negative, Nb, Zr, Hf anomalies (Parkinson and Pearce, 1998). The LILE-LREE enrichment in conjunction with HFSE depletion corroborates fluid/rock or melt/rock interactions prior to serpentization process as observed for South Sandwich arc and Tso Moriri massif (Pearce et al., 2000; Deschamps et al., 2010). The studied rocks are particularly enriched in elements which are mobile in aqueous fluids, similar to serpentinites from the Izu-Bonin- Mariana arc (Savov et al., 2005). The geochemical observations endorse selective trace element enrichment prior to serpentization, and reflects extensive metasomatism of the mantle protolith. Ti is considered as a useful tracer in identifying the protolith of serpentized ultramafic rocks. Mantle wedge peridotites, which experience extensive partial melting, have highly refractory compositions showing marked depletion in Ti (Deschamps et al., 2013). Serpentized peridotites from Mariana forearc are characterized by low bulk rock Ti (10–25 ppm; Ishii et al., 1992; Parkinson et al., 1992). The Ti contents of the studied

mantle peridotites correspond to mantle wedge serpentinites and the rocks in this study inherited their geochemical signature (MgO, Mg#, Ni, Co, Cr) from highly refractory and residual dunite in the mantle wedge after extensive melt extraction and which experienced interaction with boninitic melts during intraoceanic subduction initiation prior to serpentinization.

6.3 Mantle processes and petrogenetic implications

The trace elemental budget of subduction zone mantle peridotites reflect contribution of mantle wedge and slab derived components (Defant and Drummond, 1990; McCulloch and Gamble, 1991; Plank and Ludden, 1992; König et al., 2010). The incompatible trace element abundance patterns of the studied samples on primitive mantle normalized multi-element plots (Fig.5) depict enrichment in LILE and depletion in HFSE relative to primordial mantle compositions. This depletion in HFSE relative to fluid-mobile large ion lithophile elements is substantiated by negative Nb, Zr, Hf anomalies with respect to LILE and LREE abundances on multi-element diagrams that can be characteristically attributed to selective retention of HFSE in the subducting slab at subduction zone magmatic regime associated with typical island arc environments (Zhao et al., 1995; Ray et al., 2013). The selective enrichment of alkali and alkaline earth metals, incompatible elements like Rb, Ba, Sr, Th and relative depletion in HFSE like Nb, Ta are distinct geochemical signatures of magmas generated in subduction zone settings. The LILE enrichment in the studied rocks suggests metasomatism of a depleted MORB-type mantle by LILE rich fluids derived through the dehydration of the subducted slab and transported to the overlying mantle by fluid-transfer processes (Saunders et al., 1980; Pearce et al., 1995; Aldanmaz et al., 2008; Ganguly et al., 2016). The LREE-enriched geochemical fingerprints in the studied samples have been attributed to mantle wedge metasomatism by subduction components derived from ocean sediment and altered oceanic crust, transferred by melts or fluids derived from the subducted slab (Pearce et al., 1984; Plank and Langmuir, 1993; 1998). Therefore, the trace and rare earth element chemistry of the investigated mantle peridotites is consistent with their refractory compositions accounting for prior melt extraction and incompatible element depletion in the mantle regime with post-subduction enrichment processes contributing towards elevated LILE-LREE abundances.

The overall geochemical characteristics of the serpentinized mantle dunites from south Andaman ophiolite suite, marked by high $\text{Al}_2\text{O}_3/\text{TiO}_2$ ratios ranging from 33-100 and low $\text{CaO}/\text{Al}_2\text{O}_3$ varying between 0.01 and 0.15, U-shaped chondrite-normalized REE patterns (Fig. 5) and with LREE and HREE enrichment and relative MREE depletion at $(\text{La}/\text{Sm})_{\text{N}} > 1$ and $(\text{Gd}/\text{Yb})_{\text{N}} < 2$ collectively suggest the role of boninitic melts in their genesis. The MgO, Ni, Cr concentrations and Mg# for the studied samples invoke a refractory composition that experienced multiple episodes (~20%) of melt

extraction (Fig.9A). Fluid/melt-rock and fluid/melt-mantle interactions modify the depleted mantle restites either by percolation of sulfide melt or by refertilization by silicate melts (Luguet et al., 2003; Becker et al., 2006; Fischer-Gödde et al., 2011). Generally, harzburgites are regarded as the depleted, refractory residues produced by partial melting in the mantle; however, bulk chemical compositions of the studied south Andaman mantle dunites indicate that they have also undergone melt-rock interactions and their formation in the mantle sections of the ophiolite is ascribed to interaction between infiltrating melts and upper mantle peridotites (Kelemen and Dick,1995). This process results in the selective dissolution of pyroxene and precipitation of olivine. Dunite may form as cumulates of mafic magmas. Dunite also forms as a reaction product of primitive mafic melt with peridotites where pyroxene is replaced by olivine. Dunite may form as the result of high degrees of partial melting after fusion of clinopyroxene and orthopyroxene (Bernstein et al., 2007). Such highly refractory dunite forms through influx fusion in mantle wedges. The mantle dunites from south Andaman ophiolite suite have well-developed, U-shaped REE patterns indicating significant LREE enrichment following partial melting, although their origin as a residuum from partial melting of primitive mantle is not consistent with the observed geochemical features (Prinzhofer and Allègre, 1985; Freyet al., 1991). Tb/Yb variations with respect to Al_2O_3 for the studied samples attest to the occurrence of spinel as stable aluminous phase in the mantle residue and thus reflect shallow level partial melting of a garnet free mantle regime in the compositional domain of spinel peridotite (Fig. 9B). Prinzhofer and Allègre (1985) proposed the sequential integrated disequilibrium melting model beginning in the garnet lherzolite facies and ending in the plagioclase facies to explain the U-shaped patterns of the New Caledonian peridotites. U-shaped REE patterns are now believed to reflect partial melting coupled with melt-rock interactions as observed in other ophiolitic mantle peridotites worldwide (Xia et al., 2003; Dubois-Côté et al., 2005; Zhou et al., 2005; Polat et al.,2006; Song et al., 2009; Caran et al., 2010; Ulrich et al., 2010). It is unlikely that the melt that reacted with these mantle dunites to generate the U-shaped REE patterns had MORB compositions because MORB magmas have LREE-depleted chondrite-normalized REE patterns. However, boninites commonly possess U-shaped chondrite-normalized REE patterns (Crawford, 1989; Hickey and Frey, 1982; Falloon, 2008), resembling that of the mantle dunites from south Andaman ophiolite suite. These observations substantiate the potential of a boninitic melt which reacted with the studied mantle dunites and produced the U-shaped REE patterns observed in this study. The low-Ca boninitic compositions for the studied samples further advocate a depleted mantle source. Plots fall away from the field of impregnated, refractory, abyssal peridotites in Ni vs. Mg# diagram (Fig. 9C) and conform to refertilization of mantle wedge peridotites by boninitic melts. The LREE-enriched samples with $(La/Sm)_N > 1$ plot on HZ1-HZ2-HZ3-CC intersection curve in $(La/Sm)_N$ vs. $(1/Sm)_N$ diagram (Fig. 9D) thereby corroborating melt percolation

and re-enrichment of depleted MORB-type mantle, fluid-mantle, mantle-melt and mantle-crust interactions in SSZ setting.

Experimental studies and trace element modelling have indicated that high water contents, elevated mantle temperature and mantle decompression are the essential precursors to the generation of boninitic melts (Sobolev and Danyushevsky, 1994; Falloon and Danyushevsky, 2000; Xia et al., 2012) that are suggested to be derived through high degree of partial melting of a depleted mantle fluxed by slab-derived fluids/melts in subduction regime at high temperature (1130-1275°C), shallow depths (0.3-1.7 GPa); and under hydrous condition (Crawford et al., 1989; Defant and Drummond, 1990, Pearce et al., 1992; Manikyamba et al., 2005; 2015). Subduction of an active spreading ridge or a young oceanic slab, and initiation of subduction along transform fault in an active ridge-transform system are indicated as favourable conditions for generation of boninites. The depleted nature of mantle and unusual melting conditions at high temperature with volatile flux substantiate the melt depletion and re-enrichment processes experienced by the mantle wedge during generation of boninitic melts. The boninitic composition and associated geochemical fingerprints of the serpentinized mantle wedge dunites of the south Andaman ophiolite suite reflect intraoceanic subduction initiation, fore-arc extension and formation of spreading centre above subduction zone. The geochemical features of the studied rocks invoke multistage petrogenetic process involving the following mechanisms. (i) Multiple episodes of extraction of basaltic melt rendering a depleted, refractory upper mantle residue where $(\text{HREE})_N > (\text{MREE})_N > (\text{LREE})_N$. (ii) Intraoceanic subduction initiation ensued by downwelling of oceanic slab counter balanced by upwelling of asthenospheric mantle, thinning of the overlying lithosphere, decompression melting of a fertile, lherzolithic, asthenospheric mantle wedge giving rise to MORB-type magmas in an arc regime, leaving behind a refractory, harzburgitic mantle restite. (iii) Dehydration of subducted slab, release of fluids through slab-dehydration, which are enriched in incompatible elements (LILE, LREE) (iv) LILE and LREE enrichment of depleted mantle wedge by influx of slab-dehydrated fluids and melts causing metasomatism. (v) High-temperature, shallow level melting of metasomatized mantle wedge generating boninitic melts (vi) Interaction between mantle wedge dunite and boninitic melts. (vii) Melt percolation, melt-rocks interactions transforming mantle harzburgites to mantle dunites. (viii) Serpentinization of mantle wedge dunites by slab-dehydrated hydrous fluids.

6.4 Implications on PGE systematics

The PGE abundances of mantle-derived ultramafic-mafic rocks are controlled by (i) nature of the mantle source; (ii) previous melt extraction episodes; (iii) extent of mantle metasomatism; (iv) conditions of mantle melting including the degree and depth of partial melting; and (v) crustal

assimilation and fractional crystallization processes during the ascent and emplacement of magma (Arndt et al., 2005; Naldrett, 2010; Shellnutt, 2014; Manikyamba and Saha, 2014). Most ultramafic-mafic magmas are considered to be generated from a mantle source having peridotitic composition marked by olivine, orthopyroxene, clinopyroxene and an aluminous phase that varies with the depth of melting domain i.e. plagioclase at <0.9 GPa, spinel at 0.9-3 GPa, and garnet at >3 GPa. The minor phases that are associated with a peridotitic source mantle include hydrous silicates, carbonates, sulphides and/or PGE-rich alloy. PGE distribution in arc magmas is not only attributed to partial melting of mantle, but infiltration of fluids and hydrous metasomatism of mantle wedge collectively account for their PGE concentrations. The behaviour of highly siderophile elements (HSE) including Re, Os and PGE (Os, Ir, Ru, Rh, Pt, Pd) in boninites provide important constraints on their mobility in slab fluids and melts, melting of a metasomatised mantle wedge and the role of subduction components in genesis of arc magmas (Wood et al., 1992; Kepezhinskias et al., 2002; Dale et al., 2008; Saha et al., 2015; Singh et al., 2016).

Mantle Melting

Based on their melting temperatures, PGE are classified as the Iridium group (IPGE, Os, Ir, and Ru) having melting temperature of ~2000°C) and the Palladium group (PPGE, Rh, Pt and Pd) with melting temperature below 2000 °C) (Woodland et al., 2002). These two groups of PGEs occur within different mantle phases in peridotites or mantle rocks derived through high degrees of partial melting that removed most of the base metal sulphides (Barnes et al., 1985; Aldanmaz and Koprubasi, 2006; Mondal, 2011). PGE fractionation trends during partial melting suggest that IPGEs are more compatible, occur as discrete minerals or sulphides, alloys or oxides, often hosted within silicate grains, with their abundance increasing in the residual mantle with high degrees of partial melting. In contrast, the PPGE are relatively incompatible, occur as sulphides and alloys, often as interstitial grains with enriched PPGE in resultant melts and subchondritic Rh/Ir and Pd/Ir ratios in residual mantle after melt extraction (Barnes et al., 1985; Shirey and Walker, 1998; Alard et al., 2000; Rehkämper et al., 1999; Lorand et al., 2000). The sulfur content of primitive mantle peridotite has been estimated as 200-300 ppm with sulfide disappearing into the melt at 17 to 25 % partial melting (McDonough and Sun, 1995; Rehkämper et al., 1999). O'Neill et al. (1995) and Leshner and Stone (1996) have suggested that depleted mantle peridotite, which is the source of many mafic-ultramafic magmas, may contain as little as 125 ppm S which would require lower degrees of melting to consume all the sulfides. Melt partition co-efficient of PGEs in sulphide-silicate association is very high suggesting that magmas generated by low degree of partial melting are relatively enriched in Pd and Pt than those derived by higher degree of mantle melting (Keays, 1982; Naldrett, 1997, 2010; Herzberg et al., 2010; Luguet et al., 2001).

The mantle peridotites (dunites) in this study show characteristic higher concentrations of PGE including Pd (4.4-12.2 ppb) and Pd/Ir (2-5.5) compared to the relatively low values of Pt (2.4-12 ppb) and Pt/Pd (0.4-1.6). These features suggest contribution from slab-dehydrated fluids and hydrous melting of depleted mantle wedge under high temperatures and fluid pressure in an intraoceanic subduction setting. PGE compositions of the studied samples with relative enrichment of PPGE over IPGE, and pronounced enhancements of Pd relative to Pt provide evidence for a multi-stage petrogenetic process marked by fluid influx, mantle metasomatism and selective enrichment of incompatible and less refractory siderophile elements in the mantle environment. The elevated Pd and Au concentrations in high-Ca boninites of northern Tonga arc provide evidence for residual monosulphide solution and indicate subduction influx into the mantle source (Karrei et al., 2008). The mantle peridotites of AOB also have higher Pd and Pd/Ir ratios which suggest retention of sulphides by influx of slab-derived fluids into mantle wedge via subduction and high fluid pressure. Chondrite normalized PGE patterns of the studied mantle peridotites ($PPGE/IPGE > 1$) reflect higher degrees of mantle melting that result in PGE fractionation. The Pd and Pt contents (4.4-12.2 ppb Pd, 2-12 ppb Pt) account for higher degrees of mantle melting for the generation of parent melts. PGE compositions of the fertile primitive upper mantle is characterized by 3.5 ± 0.4 ppb Ir, 3.9 ± 0.5 ppb Os, 7.0 ± 0.9 ppb Ru, 7.6 ± 1.3 ppb Pt, 7.1 ± 1.3 ppb Pd and 1.9 ± 0.6 ppb Au (Becker et al., 2006). The IPGE and PPGE contents for the studied samples compared to the primitive mantle values suggest a depleted to enriched mantle source for their generation. The studied rocks with Pd/Ir values ranging from 2 to 5.5 correspond to higher degrees of mantle melting. On Pd/Ir vs. Ni/Cu discrimination plot (Fig. 10A) the studied samples cluster in the field for mantle. On Pd/Ir vs. Pt/Pt* plot (Fig. 10B) the studied samples correspond to the partial melting trend of asthenospheric mantle. However, it has to be noted that partial melting of mantle is not the sole factor that accounts for PGE fractionation which is also influenced by melt percolation and metasomatic processes operating in the mantle. The PGE chemistry of mantle peridotites from south Andaman ophiolite suite, as observed in this study, is marked by relative enrichment of PPGE over IPGE and pronounced enhancement of Pd/Ir relative to Pt/Pd. This feature cannot be explained by simple in situ melt extraction and removal of sulphide phases but suggest mobilization of less refractory siderophile elements, selective incompatible element enrichment of mantle, melt percolation and input from subduction-derived fluids. The enriched Ir and Ru compositions of these rocks are analogous to mantle restite. Chondrite-normalized PGE patterns for these samples suggest that they have marked enrichments in Pd with depletion in Pt which may be attributed to interaction between mantle wedge and subduction-derived fluids which mobilize Pd and retain insoluble Pt-rich sulphide phase. The percolation of slab-dehydrated fluids into the arc mantle accounts for PPGE and IPGE fractionation during mantle metasomatism. The studied samples have

lower Pt/Pd which reflect decoupling of Pt from Pd during fractional crystallization of silicates like olivine and oxides like chromite in early stages of magmatic differentiation (Crocket and Paul, 2004; Said et al., 2011).

Melt-rock interaction

PGE compositions provide important clues to identify the protoliths of serpentinized mantle peridotites. IPGE, especially Ir are not mobile during hydrothermal alteration and even during intense metasomatism (Wang et al., 2008), and are therefore good indicators for evaluating the protoliths of ultramafic rocks. The concentrations and ratios of IPGE to Pt may be used to identify the protoliths of ultramafic rocks (Guillot et al., 2001; Hattori et al., 2010). Among PPGE, Pd is mobile in hydrothermal fluids, which control enrichment and depletion of Pd in serpentinites. Most serpentinites from subduction zones contain high IPGE, similar to primitive mantle values, suggesting that these serpentinites are residual mantle peridotites. Chondrite-normalized PGE patterns for the studied mantle peridotites of south Andaman ophiolite suite are comparable with that of Northwest Anatolian peridotites and peridotites from Sumail, Zhongba, and Luqu ophiolites in terms of Ru and Pd enrichments and negative Ir anomalies (Fig. 6). The elevated abundances of Pd (4.4-12.2 ppb) with high $\sum\text{PPGE}/\sum\text{IPGE}$ (2-3) and Pd/Ir (2-5.5) ratios in the studied samples of serpentinized mantle dunites conform to extensive melt-rock interaction through percolation of boninitic melts enriched in fluid-fluxed LILE-LREE into the depleted mantle residual after several episodes of melt extraction. This boninitic geochemical imprints of the studied rocks is imparted by the infiltration of boninitic melts into the depleted and residual mantle wedge peridotite. The high Pd contents with relatively lower Ir concentrations of the samples are analogous to characteristic PGE signatures of boninitic magmas. The PGE compositions of the samples marked by higher Os and Ru concentrations corroborate higher degree of partial melting of mantle. Similar geochemical features have been observed in mantle peridotites of the Zhongba ophiolites (Dai et al., 2011). The PGE patterns of the studied samples with high Os+Ir (2-8.6 ppb) and Ru (2.8-8.4 ppb) suggest them to be rejuvenated by infiltration of melts derived by high degree partial melting of subduction-related mantle wedge. The imprints of melt-rock interaction make them geochemically comparable with Samail harzburgites from Oman ophiolite (Lorand et al., 2009) and Luobusa peridotites (Zhou et al., 2005), the Luobusa peridotites. The compositional array of the studied samples on $\sum\text{PGE}$ vs. $\sum\text{PPGE}/\sum\text{IPGE}$ plot (Fig. 10C) suggest that in terms of PGE compositions they are analogous to serpentinites of Kempirsai ophiolites from the Urals (Singh et al., 2013).

Fractional crystallization

It has been envisaged that during fractional crystallization, IPGEs (Os, Ir, Ru) are primarily concentrated in cumulus silicate minerals whereas Cu-rich interstitial sulphides mostly host PPGEs (Pd and Pt; Lorand et al., 1999; Alard et al., 2000; Said et al., 2011). Fractionation of sulphides, chromites and olivine predominantly control the concentration of Pd and Ir (Barnes et al., 1985; Lorand and Alard, 2002; Luguet et al., 2001). Sulphides enclosed in silicate phases have high Os and Ir resulting in low Pd/Ir ratios (Alard et al., 2000; Barnes et al., 1985; Naldrett, 2010). Interstitial sulphides formed by crystallization of sulphide bearing melts have low melting points whereas partial melting of silicate hosted sulphides requires higher temperatures. Increasing degree of partial melting lead to fusion of silicate enclosed sulphides and IPGE alloys producing lower Pd/Ir ratios. The IPGEs and PPGEs have different solubilities in silicate magmas. The IPGEs like Ir and Os are more refractory and compatible during mantle melting whereas PPGE are incompatible. This observation has led Pd/Ir to be considered as an effective index of PGE fractionation during petrological processes. Pd/Ir ratio increase with differentiation in magmatic fractionation and it is ~ 1 in unfractionated materials. Low Pd/Ir ratios for the studied mantle peridotite samples are attributed to (i) higher degrees of partial melting that induce fusion of IPGE forming a melt enriched in IPGE with lower Pd/Ir ratios (ii) fractional crystallization of silicate phases like olivine and chromite with high Ir and Ru. In Ni/Pd vs. Cu/Ir diagram the sample arrays define two dominant trends consistent with olivine and sulphide fractionation in the parent magma (Fig. 11A) indicating that PGE distribution in these rocks was dominantly controlled by olivine and sulphide fractionation. PGE fractionation in magmas is associated with mantle melting and crystallization processes. The studied mantle peridotites with 0.8-3.6 ppb Ir suggests partitioning of Ir into the early crystallizing mineral phases like olivine. The elevated MgO contents (35.8-42.2 wt.%) of the studied samples are consistent with lower degrees of magmatic differentiation and account for the lower Pd/Ir ratios. The high MgO mantle peridotites in this study marked by higher Ir contents and lower Pd/Ir conform to higher degrees of partial melting accompanied by Ir partitioning into early crystallizing minerals. It has been suggested that Pt/Pd ratios are significantly diminished by early fractionation of silicates, chromites, PGE and decoupling of Pt from Pd by crystal fractionation (Crocket and Paul, 2004; Said et al., 2011). The Pt/Pd ratios for these rocks (0.4-1.4) are lower than primitive mantle (1.82; McDonough and Sun, 1995) attesting to early fractionation of silicates, chromites and PGE. The Pd/Pt ratios (0.6-2.2) are higher than average Pd/Pt ratios of the mantle (0.57; Taylor and McLennan, 1985) which is attributed to PGE depletion in parent magma. It has been envisaged that PGE fractionation is largely controlled by (i) the exhaustion of sulphide in the mantle source, which is dependent on the degree of both partial melting and prior melt

depletion and (ii) the retention of IPGE in the mantle residue by platinum group minerals and Cr-spinel. The Cu, Ru, Pd, Ir and Pt concentrations for the studied samples indicate that these elements were compatible and were incorporated into early crystallizing phases like olivine.

Sulphide saturation history

PGE contents in magma are controlled by two factors: 1) sulphur solubility in the magma which is increased due to decompression leading to S-undersaturation and 2) evolution of S-undersaturated magma through crustal assimilation and fractional crystallization (AFC) which reduces sulphur solubility (Said et al., 2011). Sulphur abundance of magma is controlled by (a) degree of mantle melting where sulphur concentration decreases with increasing degree of partial melting and (b) combination of mantle metasomatism and interaction with fluids. According to Chen and Xia (2008), formation of S-saturated and S-undersaturated melts are related to the partial melting of primitive mantle. During the formation of S-saturated melts, the immiscible sulphide liquid will be separated and retained in the residual mantle resulting in a PGE-poor melt as PGE are siderophile in nature. PGE abundances vary in the order of increasing compatibility ($Ir < Ru < Pt < Au < Pd$) for the melt in sulphur undersaturated conditions (Naldrett, 2010; Barnes et al., 1985; Keays, 1995; Vogel and Keays, 1997).

The removal or incorporation of sulphides are suggested to be the key processes leading to the variation in relative PGE abundances of both melt and residual products of mantle melting (Röhkamper et al., 1999; Bennett et al., 2000; Bockrath et al., 2004). Platinum group elements are strongly chalcophile in nature owing to their high sulphide/silicate partition coefficient ranging from 10^3 - 10^5 . The distribution of PGEs in mantle derived melts is related to the solubility of sulphur in the magma (Keays and Campbell, 1981; Peach et al., 1990). Sulphur solubility in magma is reduced by decompression, crustal assimilation and fractional crystallization (AFC), which in turn result into S-undersaturation in magma (Lightfoot and Keays, 2005). The concentration of sulphur in magma decreases with increasing degree of partial melting, mantle metasomatism and interaction with fluids (Barnes et al., 1985; Naldrett, 2004; Arndt et al., 2005). At higher degree of partial melting (~25%) S-undersaturated magma is expected to form in which PGE will be retained in the mantle residue. Therefore, wide variation in relative PGE abundances of melt and residual products of mantle melting are attributed to processes associated with varying degrees of sulphide removal or incorporation in magma. During magmatic differentiation, sulphur and Cu behave similarly and therefore, Cu serves as a proxy for sulphur. Pd being the most chalcophile of all PGEs, its abundance is controlled by S-saturation and S-precipitation from a melt. Thus, the relationship between Cu and Pd has been identified as a useful indicator of the degree of S-saturation of magmas (Vogel and Keays, 1997; Woodland et al., 2002; Chen and Xia, 2008). The trace element and PGE compositions of the

studied mantle peridotites marked by Ni=25-37 ppm, Cr=39-64 ppm, Σ PGE=26.23-68.35 ppb and Σ PPGE=24.1-63.3 ppb suggest a crustally uncontaminated, sulphide unsaturated and PGE depleted character of the parent magma. The Pd and Cu relationships indicating sulphur under saturated character of the serpentinized peridotites (Fig.11B) along with their boninitic affinity suggest modification and rejuvenation of depleted mantle composition by subduction-derived fluids and boninitic melts derived through high degree partial melting.

6.5 Metasomatism and serpentinization: Subduction initiation and geochemical cycling

Serpentinites and serpentinization occurring at mid-oceanic ridge-rift systems and subduction zones provide significant clues for understanding elemental cycling and ocean-crust-mantle interplay. Serpentinites are hydrated ultramafic rocks with up to 15–16 wt.% and average of 13 wt.% H₂O content and formed through the alteration of olivine- and pyroxene-dominated ultramafic rocks at temperatures lower than 650–700°C (Evans et al., 2013). The studied mantle wedge peridotites from south Andaman ophiolite suite experienced extensive serpentinization and metasomatism thereby resulting in marked enrichments in fluid-mobile elements (FME) that are ascribed to fluid-rock interactions during subduction by percolation of fluids released from different lithologies from the dehydrating oceanic slab. Geophysical and geochemical studies of modern and ancient subduction systems have emphasized the presence of serpentinites and the role of serpentinization in subduction zone tectonics and global geochemical cycle (Deschamps et al., 2013). Experimental studies and detailed observations on geochemical database of serpentinites have suggested their hydrated nature and stability over a relatively wide P–T range and their potential as a sink of fluid mobile elements (FME) and also as an effective carrier of water to depths up to 120 to 170 km (Ulmer and Trommsdorff, 1995; Deschamps et al., 2011). Geochemical attributes of the studied serpentinized mantle peridotites provide insights into the process of fluid-induced metasomatism and serpentinization processes and their implications within island arc settings. The migration of slab-dehydrated fluids promotes mobilization of elements and contributes to 3-25% of melting of mantle wedge at a depth of 30-50 km and at 1250-1350°C mantle temperatures (Kimura and Nakajima, 2014; Plank et al., 2013). Therefore, fluid transportation from slab to mantle wedge and its role in subduction zone magmatism supports the contention that island arc tholeiites contain 1-8 wt.% of subduction derived hydrous fluids compared to the mid oceanic ridge basalts (MORB, 0.2 wt.%) and ocean island basalts (OIB, 0.8 wt.%; Saal et al., 2002; Kimura and Nakajima, 2014; Volker et al., 2014). On Nb/Zr vs. Th/Zr plot the studied samples depict a trend consistent with fluid related enrichment of mantle during the subduction process (Fig.11C).

The geochemical exchange of elements between the subducted oceanic slab and sub-arc mantle wedge, the different stages of subduction from initiation to maturation and associated melt generation processes, interaction between subduction-derived magmas and overlying arc crust, subduction-driven asthenospheric upwelling collectively account for the diverse compositional spectrum of magmas produced in the subduction factory and even those associated with subsequent rift events (Straub and Zellmer, 2012; Spandler and Pirard, 2013; Iwamori and Nakamura, 2015; Santosh et al., 2015, 2018; Yang et al., 2016). During the course of subduction, from initiation to maturation, the mantle wedge is chemically modified and enriched by the influx of hydrous fluids released by the dehydration of the downgoing oceanic crust, siliceous slab melts derived by melting of subducted slab and subduction-derived sediments which in turn serve as the most viable agents for transfer of different elements from slab to mantle wedge (Stern et al., 1990; Kimura and Yoshida, 2006; van Keken et al., 2011). These subduction-derived components eventually trigger metasomatism and flux-controlled partial melting of mantle wedge (Tatsumi, 2005; Kimura and Nakajima, 2014; Liu et al., 2015). The intraoceanic fore arc crust is either deeply submerged or the exposed ones are vulnerable to tectonic erosion which restricts their study for understanding their nature and origin (Falloon et al., 2008; Stern, 2004; Stern et al., 2012). However, drilled samples of fore-arc peridotites (upper mantle) exposed in the inner trench walls of Izu-Bonin-Mariana, Tonga and South Sandwich subduction zones provide a window to the complete crustal section at shallower depth along with the crust mantle transitional zone at Moho. The fore-arc oceanic lithosphere along with the uppermost boninitic layer further substantiates sea floor spreading during the initial stage of subduction (Crawford, 1989; Pearce et al., 1992). As the subduction progresses, the subducting slab reaches to melting stage. The relative concentrations of Nd and Hf provide important constraints in understanding the nature of subduction components in SSZ mantle melting regions. It has been suggested that the possible roles of slab-derived components like aqueous fluids released from the subducted slab during dehydration or silicate melts generated by partial melting of slab components are crucial in characterizing the geochemical signatures of subduction zone magmas (Pearce et al., 1999; Aldanmaz et al., 2008). According to the general consensus, Hf is soluble to varying degrees in siliceous melts, but, has a low solubility in aqueous fluids derived from subducted materials and does not get transported to the mantle by the fluids originated from slab dehydration (Aldanmaz et al., 2008). In contrast, Nd is more soluble in both subduction derived fluids and melts. In this case, the Nd/Hf ratios of the studied mantle peridotites ranges from 4.9-14.3 and such high values are not consistent with partial melting of subducted sediments or oceanic crust and support the contention of release of aqueous fluids through dehydration of subducted slab in making up the subduction component. Further, the high Nd/Hf and low Hf/Yb (0.2-1.00) ratios of the investigated rocks attest to their SSZ character.

A schematic diagram demonstrates the magmatic and tectonic processes involved in the evolution of serpentinized mantle wedge peridotite of south Andaman ophiolite suite (Fig. 12). The “subduction factory” at intraoceanic convergent plate margin settings is marked by the subduction of Indian plate beneath Burmese plate. Geochemical signature of the studied SSZ mantle wedge peridotites provide viable tools to understand subduction initiation and fore arc extension processes, elemental cycling and chemical variability. During the initial stages of subduction, the dehydrating oceanic slab releases hydroxyl molecules at shallow levels and mantle wedge metasomatism by influx of slab-dehydrated fluids is attributed to flux-melting and boninite magmatism. The depleted mantle wedge peridotite is refertilized by boninitic melt percolation and serpentinized by the subduction-derived fluids. The serpentinization is driven by fluids released through dehydration of subducted oceanic slab lithologies. The serpentinized mantle wedge peridotites from south Andaman ophiolite suite represent the upper mantle residue or the lowermost unit in an intraoceanic forearc section and preserve a comprehensive record of oceanic crust trapped on commencement of subduction, the magmatic and tectonic processes that were operative during subduction initiation, fore arc extension and subsequent oceanic crust generation in a SSZ environment. Therefore, we envisage (Fig.12) that the boninitic feature of the mantle wedge peridotites from south Andaman ophiolite attests to the following processes; (i) Fore arc lithospheric extension and asthenospheric upwelling in response to subduction initiation in a SSZ setting (ii) Fluid-transfer from subducted slab to mantle wedge, metasomatism and flux-melting (iii) Interaction between boninitic melts and depleted MORB-type mantle wedge (iv) Refertilization of refractory mantle peridotite of harzburgite-dunite assemblages by boninitic melts. The geochemical and tectonic attributes in this study provide evidence for metasomatism, serpentinization and refertilization of depleted mantle wedge peridotite during initiation and fore arc extension in SSZ settings of Phanerozoic intraoceanic arc systems and geochemical cycling at SSZ through ocean-crust-mantle interaction.

7. Conclusions

- The serpentinized dunites with relict olivine in the Badmash pahar area of south Andaman represent the tectonized mantle section of south Andaman ophiolite suite.
- The dunitic protolith point corresponds to restitic mantle peridotite which was subjected to extensive melt extraction.
- Geochemical features marked by LILE-LREE enrichment, HFSE depletion, and U-shaped chondrite-normalized REE patterns suggest multistage petrogenetic processes including

refertilization of a depleted, refractory mantle wedge by subduction-derived fluids and melts operative in an intraoceanic fore-arc environment.

- The distinct boninitic signature in conjunction with trace, rare earth and PGE compositions is in accord with subduction initiation with subsequent slab roll-back triggering extension and seafloor spreading in the upper plate of intraoceanic fore-arc regime collectively endorsing a suprasubduction zone (SSZ) setting.
- This boninitic imprint of the studied rocks with distinct PGE patterns characterized by high Os+Ir (2-8.6 ppb) and Ru (2.8-8.4 ppb), elevated abundances of Pd (4.4-12.2 ppb) with high $\Sigma\text{PPGE}/\Sigma\text{IPGE}$ (2-3) and Pd/Ir (2-5.5) conform to extensive melt-rock interaction through infiltration of boninitic melts, derived by high degree of mantle melting and enriched in fluid-fluxed LILE-LREE into the depleted and residual mantle wedge peridotite at initial stage of intraoceanic subduction.
- Petrogenetic evolution is marked by hydration, metasomatism and serpentinization of depleted, MORB-type, sub-arc wedge mantle residual after repeated melt extraction episodes by fluids released from dehydrated subducted slab and refertilization of refractory mantle peridotite by boninitic melts derived at initial stage of intraoceanic subduction.
- Serpentinized and metasomatized mantle wedge dunites from south Andaman ophiolite suite record both MOR and intraoceanic arc signatures collectively suggesting SSZ affinity and represent ocean-crust-mantle interaction and associated geochemical cycling.

Acknowledgements

Abhishek Sahais grateful to the Director, CSIR-National Institute of Oceanography and Head, Geological Oceanography Division, CSIR-National Institute of Oceanography for their encouragement, support and permission to publish this work. The authors thank the handling Associate Editor and two reviewers for their insightful suggestions which have greatly improved the quality of the manuscript. The authors are thankful to Dr. M. Satyanarayanan and Dr. K.S.V. Subramanyam for providing the PGE data. AS acknowledges the funds from Council of Scientific and Industrial Research (CSIR) to CSIR-National Institute of Oceanography through the MLP-1703 project. M. Santosh is supported by Foreign Expert funding from CUGB and Professorial position at the Adelaide University. This is NIO's contribution No. XXXX.

References

- Abdel Al. A. M., Ali, S., Helmy, H. M., El-Shafei, S. A., 2016. A fore-arc setting of the Gerf ophiolite, Eastern Desert, Egypt: Evidence from mineral chemistry and geochemistry of ultramafites. *Lithos* 263, 52-65.
- Alard, O., Griffin, W. L., Lorand, J.-P., Jackson, S. E., O'Reilly, S.Y., 2000. Non-chondritic distribution of the highly siderophile elements in mantle sulfides. *Nature* 407, 891–894.
- Aldanmaz, E., Koprubasi, N., 2006. Platinum-Group-Element Systematics of Peridotites from Ophiolite Complexes of Northwest Anatolia, Turkey: Implications for Mantle Metasomatism by Melt Percolation in a Supra-subduction Zone Environment. *International Geology Review* 48, 420-442.
- Aldanmaz, E., Schmidt, M. W., Gourgaud, A., Meisel, T. 2009. Mid-ocean ridge and supra-subduction geochemical signatures in spinel–peridotites from the Neotethyanophiolites in SW Turkey: Implications for upper mantle melting processes. *Lithos* 113, 691-708.
- Aldanmaz, E., Yaliniz, M. K., Güctekin, A., Göncüoğlu, M. C. 2008. Geochemical characteristics of mafic lavas from the Neotethyanophiolites in western Turkey: implications for heterogeneous source contribution during variable stages of ocean crust generation. *Geological Magazine* 145, 37-54.
- Arndt, N.T., C.M. Lesher C.M., Czamanske, G.K., 2005. Mantle-derived magmas and magmatic Ni-Cu-(PGE) deposits. *Economic Geology*, 100th Anniversary volume, 5-24.
- Azer, M. K., Khalil, A. E. S., 2005. Petrological and mineralogical studies of Pan-African serpentinites at Bir Al-Edeid area, central Eastern Desert, Egypt. *Journal of African Earth Sciences* 43, 525-536.
- Balaram, V., 2008. Recent advances in the determination of PGE in exploration studies-A Review. *Journal of Geological Society of India* 72, 661-677.
- Balaram, V., Mathur, R., Banakar, V. K., Hein, J. R., Rao, C. R. M., Rao, T. G., Dasaram, B., 2006. Determination of the platinum–group elements (PGE) and gold (Au) in manganese nodule reference samples by nickel sulfide fire-assay and Te coprecipitation with ICP-MS. *Indian Journal of Marine Sciences* 35, 7-16.
- Bandopadhyay, P. C., 2005. Discovery of abundant pyroclasts in the Namunagarh Grit, South Andaman: evidence for arc volcanism and active subduction during the Palaeogene in the Andaman area. *Journal of Asian Earth Sciences* 25, 95-107.
- Barnes, S.-J., 1990. The use of metal ratios in prospecting for a platinum group element deposit. *Journal of Exploration Geochemistry* 37, 91-99.
- Barnes, S.-J., Naldrett, A. J., Gorton, M. P., 1985. The origin of the fractionation of platinum-group elements in terrestrial magmas. *Chemical Geology* 53, 303–323.
- Barth, M. G., Mason, P. R., Davies, G. R., Drury, M. R., 2008. The Othris Ophiolite, Greece: a snapshot of subduction initiation at a mid-ocean ridge. *Lithos* 100, 234-254.

- Barth, M. G., Mason, P. R., Davies, G. R., Dijkstra, A. H., Drury, M. R., 2003. Geochemistry of the Othris ophiolite, Greece: evidence for refertilization?. *Journal of Petrology* 44, 1759-1785.
- Becker, H., Horan, M. F., Walker, R. J., Gao, S., Lorand, J. P., Rudnick, R. L., 2006. Highly siderophile element composition of the Earth's primitive upper mantle: constraints from new data on peridotite massifs and xenoliths. *Geochimica et Cosmochimica Acta* 70, 4528-4550.
- Bédard, É., Hébert, R., Guilmette, C., Lesage, G., Wang, C. S., Dostal, J., 2009. Petrology and geochemistry of the Saga and Sangsang ophiolitic massifs, Yarlung Zangbo Suture Zone, Southern Tibet: evidence for an arc-back-arc origin. *Lithos* 113, 48-67.
- Bennett, V. C., Norman, M. D., Garcia, M. O., 2000. Rhenium and platinum group element abundances correlated with mantle source components in Hawaiian picrites: sulfides in the plume. *Earth and Planetary Science Letters* 183, 513-526.
- Bezard, R., Hébert, R., Wang, C., Dostal, J., Dai, J., Zhong, H., 2011. Petrology and geochemistry of the Xiugugabu ophiolitic massif, western Yarlung Zangbo suture zone, Tibet. *Lithos* 125, 347-367.
- Bockrath, C., Ballhaus, C., Holzheid, A., 2004. Stabilities of laurite RuS₂ and monosulfide liquid solution at magmatic temperature. *Chemical Geology* 208, 265-271.
- Bodinier, J. L., Dupuy, C., Dostal, J., 1988. Geochemistry and petrogenesis of Eastern Pyrenean peridotites. *Geochimica et Cosmochimica Acta* 52, 2893-2907.
- Bodinier, J. L., Godard, M. 2003. Orogenic, ophiolitic, and abyssal peridotites. *Treatise on geochemistry* 2, 568.
- Bonatti, E., Michael, P. J., 1989. Mantle peridotites from continental rifts to ocean basins to subduction zones. *Earth and Planetary Science Letters* 91, 297-311.
- Bouilhol, P., Burg, J. P., Bodinier, J. L., Schmidt, M. W., Dawood, H., Hussain, S. 2009. Magma and fluid percolation in arc to forearc mantle: evidence from Sapat (Kohistan, Northern Pakistan). *Lithos* 107, 17-37.
- Caran, Ş., Çoban, H., Flower, M. F., Ottley, C. J., Yılmaz, K. 2010. Podiform chromitites and mantle peridotites of the Antalya ophiolite, Isparta Angle (SW Turkey): implications for partial melting and melt-rock interaction in oceanic and subduction-related settings. *Lithos* 114, 307-326.
- Chakraborty, P. P., Pal, T. 2001. Anatomy of a forearc submarine fan: Upper Eocene—Oligocene Andaman Flysch Group, Andaman Islands, India. *Gondwana Research* 4, 477-486.
- Chen, G., Xia, B., 2008. Platinum-group elemental geochemistry of mafic and ultramafic rocks from the Xigaze ophiolite, southern Tibet. *Journal of Asian Earth Science* 32, 406-422.
- Coleman, R. G. 1984. The Tihama Asir igneous complex, a passive margin ophiolite. In *Proceedings of the 27th International Geological Congress, Moscow*, 23, 221-239
- Coleman, R. G., 1977. What is an Ophiolite?. In *Ophiolites* (pp. 1-7). Springer Berlin Heidelberg.
- Crawford, A. J., 1989. *Boninites and Related Rocks*. Unwin Hyman, London, 465.

- Crawford, A.J., Falloon, T.J., Green, D.H., 1989. Classification, petrogenesis and tectonic setting of boninites. In: Crawford, A.J. (Ed.), *Boninites and related rocks*. Unwin-Hyman, London, pp. 1-49.
- Crocket, J.H., Paul, D.K., 2004. Platinum-group elements in Deccan mafic rocks: a comparison of suites differentiated by Ir content. *Chemical Geology* 208, 273-291.
- Currie, B. S., Rowley, D. B., Tabor, N. J., 2005. Middle Miocene paleoaltimetry of southern Tibet: Implications for the role of mantle thickening and delamination in the Himalayan orogen. *Geology* 33, 181-184.
- Dai, J. G., Wang, C. S., Hébert, R., Santosh, M., Li, Y. L., Xu, J. Y., 2011. Petrology and geochemistry of peridotites in the Zhongba ophiolite, Yarlung Zangbo Suture Zone: implications for the Early Cretaceous intra-oceanic subduction zone within the Neo-Tethys. *Chemical Geology* 288, 133-148.
- Dale, C. W., Luguet, A., Macpherson, C. G., Pearson, D. G., Hickey-Vargas, R., 2008. Extreme platinum-group element fractionation and variable Os isotope compositions in Philippine Sea Plate basalts: tracing mantle source heterogeneity. *Chemical Geology* 248, 213-238.
- Defant, M. J., Drummond, M. S., 1990. Derivation of some modern arc magmas by melting of young subducted lithosphere. *Nature* 347, 662-665.
- Deschamps, F., Godard, M., Guillot, S., Hattori, K., 2013. Geochemistry of subduction zone serpentinites: A review. *Lithos* 178, 96-127.
- Deschamps, F., Guillot, S., Godard, M., Chauvel, C., Andreani, M., Hattori, K., 2010. In situ characterization of serpentinites from forearc mantle wedges: timing of serpentinization and behavior of fluid-mobile elements in subduction zones. *Chemical Geology* 269, 262-277.
- Deschamps, F., Kaminski, E., Tackley, P. J., 2011. A deep mantle origin for the primitive signature of ocean island basalt. *Nature Geoscience* 4, 879.
- DeShon, H. R., Schwartz, S. Y., 2004. Evidence for serpentinization of the forearc mantle wedge along the Nicoya Peninsula, Costa Rica. *Geophysical research letters* 31.
- Dilek, Y., Furnes, H., 2009. Structure and geochemistry of Tethyan ophiolites and their petrogenesis in subduction rollback systems. *Lithos* 113, 1-20.
- Dilek, Y., 2003. Ophiolite concept and its evolution. *Special Papers-Geological Society of America*, 1-16.
- Dilek, Y., Furnes, H. 2011. Ophiolite genesis and global tectonics: geochemical and tectonic fingerprinting of ancient oceanic lithosphere. *Geological Society of America Bulletin* 123, 387-411.
- Dilek, Y., Furnes, H. 2014. Ophiolites and their origins. *Elements* 10, 93-100.
- Dilek, Y., Furnes, H., Shallo, M. 2007. Suprasubduction zone ophiolite formation along the periphery of Mesozoic Gondwana. *Gondwana Research*, 453-475

- Dilek, Y., Furnes, H., Shallo, M., 2008. Geochemistry of the Jurassic Mirdita Ophiolite (Albania) and the MORB to SSZ evolution of a marginal basin oceanic crust. *Lithos* 100, 174-209.
- Dilek, Y., Thy, P., Hacker, B., Grundvig, S. 1999. Structure and petrology of Tauride ophiolites and mafic dike intrusions (Turkey): Implications for the Neotethyan ocean. *Geological Society of America Bulletin* 111, 1192-1216.
- Dubois-Côté, V., Hébert, R., Dupuis, C., Wang, C. S., Li, Y. L., Dostal, J., 2005. Petrological and geochemical evidence for the origin of the Yarlung Zangbo ophiolites, southern Tibet. *Chemical Geology* 214, 265-286.
- Evans, B. W., Hattori, K., Baronnet, A., 2013. Serpentinite: what, why, where?. *Elements* 9, 99-106.
- Falloon, T.J., Danyushevsky, L.V., 2000. Melting of refractory mantle at 1.5, 2 and 2.5 GPa under anhydrous and H₂O-undersaturated conditions: implications for high-Ca boninites and the influence of subduction components on mantle melting. *Journal of Petrology* 41, 257–283.
- Falloon, T.J., Danyushevsky, L.V., Crawford, A.J., Meffre, S., Woodhead, J.D., Bloomer, S.H., 2008. Boninites and adakites from the northern termination of the Tonga trench: implications for adakite petrogenesis. *Journal of Petrology* 49, 697-715.
- Fischer-Gödde, M., Becker, H., Wombacher, F., 2011. Rhodium, gold and other highly siderophile elements in orogenic peridotites and peridotite xenoliths. *Chemical Geology*, 280(3), 365-383.
- Ganguly, S., Manikyamba, C., Saha, A., Lingadevaru, M., Santosh, M., Rambabu, S., Khelen, A.C., Purushotham, D., Linga, D., 2016. Geochemical characteristics of gold bearing boninites and banded iron formations from Shimoga greenstone belt, India: Implications for gold genesis and hydrothermal processes in diverse tectonic settings. *Ore Geology Reviews* 73, 59-82.
- Garuti, G., Fershtater, G., Bea, F., Montero, P., Pushkarev, E. V., Zaccarini, F., 1997. Platinum-group elements as petrological indicators in mafic-ultramafic complexes of the central and southern Urals: preliminary results. *Tectonophysics* 276, 181-194.
- Ghosh, B., Pal, T., Bhattacharya, A., Das, D., 2009. Petrogenetic implications of ophiolitic chromite from Rutland Island, Andaman—a boninitic parentage in supra-subduction setting. *Mineralogy and Petrology* 96, 59-70.
- Ghosh, B., Morishita, T., Bhatta, K., 2013. Significance of chromian spinels from the mantle sequence of the Andaman ophiolite, India: paleogeodynamic implications. *Lithos* 164, 86-96.
- Ghosh, B., Bhatta, K., 2014. Podiform chromitites in lherzolitic mantle rocks (Andaman ophiolite, India): the role of magma/rock interaction and parental melt composition. *Bulletin de la Societe Geologique de France* 185, 123-130.
- Ghosh, B., Bandyopadhyay, D., Morishita, T. 2017. Andaman–Nicobar Ophiolites, India: origin, evolution and emplacement. *Geological Society, London, Memoirs* 47, 95-110.
- Guillot, S., Hattori, K. H., de Sigoyer, J., 2000. Mantle wedge serpentinization and exhumation of eclogites: insights from eastern Ladakh, northwest Himalaya. *Geology* 28, 199-202.

- Guillot, S., Hattori, K. H., de Sigoyer, J., Nagler, T., Auzende, A. L., 2001. Evidence of hydration of the mantle wedge and its role in the exhumation of eclogites. *Earth and Planetary Science Letters* 193, 115-127
- Haldar, D. 1984. Some aspects of the Andaman Ophiolite Complex. *Rec. Geol. Surv. India* 119, 1–11.
- Hall, R., 2002. Cenozoic geological and plate tectonic evolution of SE Asia and the SW Pacific: computer-based reconstructions, model and animations. *Journal of Asian Earth Sciences* 20, 353-434.
- Hattori, K. H., Guillot, S., 2003. Volcanic fronts form as a consequence of serpentinite dehydration in the forearc mantle wedge. *Geology* 31, 525-528.
- Hattori, K., Wallis, S., Enami, M., Mizukami, T., 2010. Subduction of mantle wedge peridotites: Evidence from the Higashi-akaishi ultramafic body in the Sanbagawa metamorphic belt. *Island Arc* 19, 192-207.
- Herzberg, C., Condie, K., Korenaga, J., 2010 Thermal history of the Earth and its petrological expression. *Earth and Planetary Science Letters* 292, 79–88.
- Hickey, R. L., Frey, F. A., 1982. Geochemical characteristics of boninite series volcanics: implications for their source. *Geochimica et Cosmochimica Acta* 46, 2099-2115.
- Hoatson, D.M., Keays, R.R., 1989. Formation of platiniferous sulfide horizons by crustal fractionation and magma mixing in the Munni Munni Layered intrusion, West Pilbara Block, West Australia. *Economic Geology* 84, 117-1804.
- Ishii, T., Robinson, P.T., Maekawa, H., Fiske, R., 1992 Petrological studies of peridotites from diapiric serpentinite seamounts in the Izu±Ogasawara±Mariana forearc, Leg 125. In: Fryer P, Pearce JA, Stokking LB et al. (eds) *Proc ODP Sci Results 125, Ocean Drilling Program*, College Station, Texas, pp 445-486.
- Ishikawa, A., Kaneko, Y., Kadarusman, A., Ota, T. 2007. Multiple generations of forearc mafic–ultramafic rocks in the Timor–Tanimbar ophiolite, eastern Indonesia. *Gondwana Research* 11, 200-217
- Ishikawa, T., Nagaishi, K., and Umino, S., 2002. Boninitic volcanism in the Oman ophiolite: Implications for thermal conditions during transition from spreading ridge to arc. *Geology* 30, 899–902.
- Iwamori, H., Nakamura, H., 2015. Isotopic heterogeneity of oceanic, arc and continental basalts and its implications for mantle dynamics. *Gondwana Research* 27, 1131-1152.
- Jafri, S. H., Balaram, V., Ramesh, S. L., 1990. Geochemistry of Andaman-Nicobar island basalts: a case for a possible plume origin. *Journal of Volcanology and Geothermal Research* 44, 339-347
- Kapsiotis, A. N., 2013. Origin of mantle peridotites from the Vourinos Ophiolite Complex, Greece, as deduced from Cr-spinel morphological and chemical variations. *Journal of Geosciences* 58, 217.
- Karipi, S., Tsikouras, B., Hatzipanagiotou, K. 2006. The petrogenesis and tectonic setting of ultramafic rocks from Iti and Kallidromon Mountains, continental Central Greece: vestiges of the Pindosocean. *The Canadian Mineralogist* 44, 267-287

- Karrei, L.I., Mungall, J.E., Jenner, F., Arculus, R.J., Mavrogenes, J.A., 2008. Elevated Pt, Pd and Au concentrations in high-Ca boninites, northern Tonga arc: evidence for residual monosulphide solid solution. *Geophysical Research Abstracts* 10, EGU 2008-A-04326.
- Keays, R. R., 1982. Palladium and iridium in komatiites and associated rocks: Application to petrogenetic problems, in Arndt, N. T., and Nisbet, E. G., eds., *Komatiites*: London, George Allen and Unwin, p. 435-458.
- Keays, R. R., 1995. The role of komatiitic and picritic magmatism and S-saturation in the formation of ore deposits. *Lithos* 34, 1–18.
- Keays, R.R., Campbell, I.H., 1981. Precious metals in the Jimberlana Intrusion, Western Australia: Implications for the genesis of platiniferous ores in layered intrusions. *Economic Geology* 76, 1118-1141.
- Kelemen, P. B., Dick, H. J., 1995. Focused melt flow and localized deformation in the upper mantle: Juxtaposition of replacive dunite and ductile shear zones in the Josephine peridotite, SW Oregon. *Journal of Geophysical Research: Solid Earth* 100, 423-438.
- Kelemen, P. B., Dick, H. J., Quick, J. E. 1992. Formation of harzburgite by pervasive melt/rock reaction in the upper mantle. *Nature* 358, 635-641
- Kelemen, P. B., Rilling, J. L., Parmentier, E. M., Mehl, L., & Hacker, B. R., 2003. Thermal structure due to solid-state flow in the mantle wedge beneath arcs. *Inside the subduction factory*, 293-311.
- Kepezhinskas, P., Defant, M.J., Widom, E., 2002. Abundance and distribution of PGE and Au in the island-arc mantle: implications for sub-arc metasomatism. *Lithos* 60, 113-128.
- Kimura, J., Yoshida, T., 2006. Contributions of slab fluid, mantle wedge and crust to the origin of quaternary lavas in the NE Japan arc. *Journal of Petrology* 47, 2185–2232.
- Kimura, J-I., Nakajima, J., 2014. Behaviour of subducted water and its role in magma genesis in the NE Japan arc: A combined geophysical and geochemical approach. *Geochimica et Cosmochimica Acta* 143, 165-188.
- König, S., Munker, C., Schuth, S., Luguët, A., Hoffmann, J.E., Kuduon, J., 2010. Boninites as windows into trace element mobility in subduction zones. *Geochimica et Cosmochimica Acta* 74, 684-704.
- Korenaga, J., Karato, S. I., 2008. A new analysis of experimental data on olivine rheology. *Journal of Geophysical Research: Solid Earth* 113, B02403.
- Krishna, A.K., Murthy, N.N., Govil, P.K., 2007. Multielement Analysis of Soils by Wavelength-Dispersive X-ray Fluorescence Spectrometry. *Atomic Spectrometry* 28, 202-212.
- Leblanc, M., 1991. Platinum-group elements and gold in ophiolitic complexes: distribution and fractionation from mantle to oceanic floor. In *Ophiolite Genesis and Evolution of the Oceanic Lithosphere*, Springer, Netherlands, pp. 231-260.
- Li, Y., Yang, J., Dilek, Y., Zhang, J., Pei, X., Chen, S., ..., Li, J. 2015. Crustal architecture of the Shangdan suture zone in the early Paleozoic Qinling orogenic belt, China: record of subduction initiation and backarc basin development. *Gondwana Research* 27, 733-744

- Lightfoot, P.C., Keays, R.R., 2005. Siderophile and chalcophile metal variations in flood basalts from the Siberian Trap, Noril'sk region: implication for the origin of the Ni-Cu-PGE sulphide ores. *Economic Geology* 100, 439-462.
- Liu, F., Yang, J. S., Dilek, Y., Xu, Z. Q., Xu, X. Z., Liang, F. H., ..., Lian, D. Y., 2015. Geochronology and geochemistry of basaltic lavas in the Dongbo and Purang ophiolites of the Yarlung-Zangbo Suture zone: Plume-influenced continental margin-type oceanic lithosphere in southern Tibet. *Gondwana Research* 27, 701-718.
- Lorand, J. P., Schmidt, G., Palme, H., Kratz, K. L., 2000. Highly siderophile element geochemistry of the Earth's mantle: new data for the Lanzo (Italy) and Ronda (Spain) orogenic peridotite bodies. *Lithos* 53, 149-164.
- Lorand, J. P., Alard, O., Godard, M., 2009. Platinum-group element signature of the primitive mantle rejuvenated by melt-rock reactions: evidence from Sumail peridotites (Oman Ophiolite). *Terra Nova* 21, 35-40.
- Lorand, J. P., Pattou, L., Gros, M., 1999. Fractionation of platinum-group elements and gold in the upper mantle: a detailed study in Pyrenean orogenic lherzolites. *Journal of Petrology* 40, 957-981.
- Lorand, J.P., Alard, O., 2001. Platinum-group element abundances in the upper mantle: new constraints from in situ and whole-rock analyses of Massif Central xenoliths (France). *Geochimica et Cosmochimica Acta* 65, 2789-2806.
- Luguet, A., Lorand, J. P., Seyler, M., 2003. Sulfide petrology and highly siderophile element geochemistry of abyssal peridotites: A coupled study of samples from the Kane Fracture Zone (45 W 23 20N, MARK area, Atlantic Ocean). *Geochimica et Cosmochimica Acta* 67, 1553-1570.
- Luguet, A., Alard, O., Lorand, J. P., Pearson, N. J., Ryan, C., O'Reilly, S. Y., 2001. Laser-ablation microprobe (LAM)-ICPMS unravels the highly siderophile element geochemistry of the oceanic mantle. *Earth and Planetary Science Letters* 189, 285-294.
- Manikyamba, C., Naqvi, S. M., Rao, D. S., Mohan, M. R., Khanna, T. C., Rao, T. G., & Reddy, G. L. N., 2005. Boninites from the Neoproterozoic Gadwal greenstone belt, Eastern Dharwar craton, India: implications for Archean subduction processes. *Earth and Planetary Science Letters* 230, 65-83.
- Manikyamba, C., Ray, J., Ganguly, S., Singh, M. R., Santosh, M., Saha, A., Satyanarayanan, M., 2015. Boninitic metavolcanic rocks and island arc tholeiites from the Older Metamorphic Group (OMG) of Singhbhum Craton, eastern India: Geochemical evidence for Archean subduction processes. *Precambrian Research* 271, 138-159.
- Manikyamba, C., Saha, A., 2014. PGE geochemistry of komatiites from Neoproterozoic Sigegudda greenstone terrane, western Dharwar Craton, India. In *Proceedings of the Workshop on Magmatic Ore Deposits*. Geol. Soc. India, Special Publ. 2, 162-174.

- Manikyamba, C., Kerrich, R., Polat, A., Saha, A., 2013. Geochemistry of two stratigraphically-related ultramafic (komatiite) layers from the Neoproterozoic Sigegudda greenstone terrane, western Dharwar Craton, India: evidence for compositional diversity in Archean mantle plumes. *Lithos* 177, 120-135.
- Marchesi, C., Garrido, C. J., Godard, M., Belley, F., Ferré, E. 2009. Migration and accumulation of ultra-depleted subduction-related melts in the Massif du Sud ophiolite (New Caledonia). *Chemical Geology* 266, 171-186.
- McCulloch, M.T., Gamble, J.A., 1991. Geochemical and geodynamical constraints on subduction zone magmatism. *Earth and Planetary Science Letters* 102, 358-374.
- McDonough, W.F., Sun, S.S., 1995. The composition of the earth. *Chemical Geology* 120, 223-253.
- McDonough, W.F., Frey, F.A., 1989. REE in upper mantle rocks. In: *Geochemistry and mineralogy of rare Earth elements*. Lipin, B. and McKay, G.R. (Eds.), Mineralogical Society of America, Chelsea, Michigan, 99-145.
- Melcher, F., Grum, W., Thalhammer, T. V., Thalhammer, O. A. R., 1999. The giant chromite deposits at Kempirsai, Urals: constraints from trace element (PGE, REE) and isotope data. *Mineralium Deposita* 34, 250-272.
- Moghadam, H. S., Corfu, F., Chiaradia, M., Stern, R. J., Ghorbani, G., 2014. Sabzevar Ophiolite, NE Iran: Progress from embryonic oceanic lithosphere into magmatic arc constrained by new isotopic and geochemical data. *Lithos* 210, 224-241.
- Mondal, S.K., 2011. Platinum Group Element (PGE) Geochemistry to understand the Chemical Evolution of the Earth's Mantle. *Journal of Geological Society of India* 77, 295-302.
- Monsef, I., Rahgoshay, M., Mohajjel, M., Moghadam, H. S., 2010. Peridotites from the Khoy Ophiolitic Complex, NW Iran: Evidence of mantle dynamics in a supra-subduction-zone context. *Journal of Asian Earth Sciences* 38, 105-120.
- Naldrett, A. J., 1997. The composition of Fe–Ni–Cu–S ores as a consequence of the equilibration of sulfide liquid with silicate magma and subsequent fractional crystallization. Abstract, *Origin and fractionation of HSE in the Earth's Mantle*, vol. 59, EAG Workshop, Max-Planck-Institut für Chemie, Mainz, Germany.
- Naldrett, A. J., 2004, *Magmatic Sulfide Deposits: Geology, Geochemistry, and Exploration*, Springer, Heidelberg, 727 pp.
- Naldrett, A. J., 2010. Secular variation of magmatic sulfide deposits and their source magmas. *Economic Geology* 105, 669–688.
- Niu, Y., 2004. Bulk-rock major and trace element compositions of abyssal peridotites: implications for mantle melting, melt extraction and post-melting processes beneath mid-ocean ridges. *Journal of Petrology* 45, 2423-2458.
- O'Neill, H. S. C., Dingwell, D. B., Borisov, A., Spettel, B., Palme, H., 1995. Experimental petrochemistry of some highly siderophile elements at high temperatures, and some implications for core formation and the mantle's early history. *Chemical Geology* 120, 255-273.

- Pagé, P., Bédard, J. H., Tremblay, A. 2009. Geochemical variations in a depleted fore-arc mantle: the Ordovician Thetford Mines Ophiolite. *Lithos*, 113, 21-47.
- Pal, T., Bhattacharya, A., 2010. Greenschist-facies sub-ophiolitic metamorphic rocks of Andaman Islands, Burma–Java subduction complex. *Journal of Asian Earth Sciences* 39, 804-814.
- Pal, T., Chakraborty, P. P., Gupta, T. D., Singh, C. D. 2003. Geodynamic evolution of the outer-arc–forearc belt in the Andaman Islands, the central part of the Burma–Java subduction complex. *Geological Magazine* 140, 289-307.
- Pal, T., Gupta, T. D., Chakraborty, P. P., Gupta, S. C. D. 2005. Pyroclastic deposits of mio-pliocene age in the Arakan Yoma-Andaman-Java subduction complex, Andaman Islands, bay of Bengal, India. *Geochemical Journal* 39, 69-82.
- Palme, H., O'Neill, H. S. C., 2003. Cosmochemical estimates of mantle composition. *Treatise on geochemistry*, 2, 568.
- Parkinson, I. J., Pearce, J. A. 1998. Peridotites from the Izu–Bonin–Mariana forearc (ODP Leg 125): evidence for mantle melting and melt–mantle interaction in a supra-subduction zone setting. *Journal of Petrology*, 39, 1577-1618
- Peach, C. L., Mathez, E. A., Keays, R. R., 1990. Sulfide melt– silicate melt distribution coefficients for noble metals and other chalcophile elements as deduced from MORB: implications for partial melting. *Geochimica et Cosmochimica Acta* 54, 3379–3389.
- Pearce, J. A. 2003. Supra-subduction zone ophiolites: the search for modern analogues. *Special Papers-Geological Society of America*, 269-294.
- Pearce, J. A., Robinson, P. T. 2010. The Troodosophiolitic complex probably formed in a subduction initiation, slab edge setting. *Gondwana Research* 18, 60-81
- Pearce, J. A., Baker, P. E., Harvey, P. K., Luff, I. W., 1995. Geochemical evidence for subduction fluxes, mantle melting and fractional crystallization beneath the South Sandwich island arc. *Journal of Petrology* 36, 1073-1109.
- Pearce, J. A., Barker, P. F., Edwards, S. J., Parkinson, I. J., Leat, P. T., 2000. Geochemistry and tectonic significance of peridotites from the South Sandwich arc–basin system, South Atlantic. *Contributions to Mineralogy and Petrology* 139, 36-53.
- Pearce, J. A., Lippard, S. J., Roberts, S., 1984. Characteristics and tectonic significance of supra-subduction zone ophiolites. *Geological Society, London, Special Publications* 16, 77-94.
- Pearce, J.A., Sieger, R. Arculus, R.C., Murton, B.J., Ishii, T., Peate, D.W., Paerkinson, I. J., 1992. Boninite and Harzburgite from Leg 125 (Bonin-Mariana Forearc): A case study of magma genesis during the initial stages of subduction. *Proceedings of the Ocean Drilling Program Scientific Results* 125, pp. 623-659.
- Pearson, D. G., Canil, D., Shirey, S. B., 2003. Mantle samples included in volcanic rocks: xenoliths and diamonds. *Treatise on geochemistry* 2, 568.
- Plank, T., Kelley, K.A., Zimmer, M.M., Hauri, E.H., Wallace, P.J., 2013. Why do mafic arc magmas contain ~4% water on average? *Earth and Planetary Science Letters* 364, 168-179.

- Plank, T., Langmuir, C. H., 1993. Tracing trace elements from sediment input to volcanic output at subduction zones. *Nature* 362, 739-743.
- Plank, T., Langmuir, C.H., 1998. The chemical composition of subducting sediments and its consequences for the crust and mantle. *Chemical Geology* 145, 325-394.
- Plank, T., Ludden, J. N., 1992. Geochemistry of sediments in the Argo Abyssal Plain at Site 765: A continental margin reference section for sediment recycling in subduction zones. *Proceedings of the Ocean Drilling Program - Scientific Results* 123, 167 – 189.
- Polat, A., Herzberg, C., Münker, C., Rodgers, R., Kusky, T., Li, J., Delaney, J., 2006. Geochemical and petrological evidence for a suprasubduction zone origin of Neoproterozoic (ca. 2.5 Ga) peridotites, central orogenic belt, North China craton. *Geological Society of America Bulletin* 118, 771-784.
- Prinzhofer, A., Allègre, C. J. 1985. Residual peridotites and the mechanisms of partial melting. *Earth and Planetary Science Letters* 74, 251-265.
- Ray, J., Saha, A., Koeberl, C., Thoni, M., Ganguly, S., Hazra, S., 2013. Geochemistry and petrogenesis of Proterozoic mafic rocks from east Khasi Hills, Shillong Plateau, northeastern India. *Precambrian Research* 230, 119-137.
- Ray, K. K., Sengupta, S., Van den Hul, H. J. 1988, Chemical characters of volcanic rocks from Andaman Ophiolite, India. *Journal of the Geological Society of London*, 145, 392–400.
- Röhkamper, M., Halliday, A.N., Fitton, J., Alt, J., Takazawa, E., 1999. Non-chondritic platinum-group element ratios in oceanic mantle lithosphere: Petrogenetic signature of melt percolation?. *Earth and Planetary Science Letters* 172, 65-81.
- Robertson, A. H. 2002. Overview of the genesis and emplacement of Mesozoic ophiolites in the Eastern Mediterranean Tethyan region. *Lithos* 65, 1-67.
- Saal, A.E., Hauri, E.H., Langmuir, C.H., Perfit, M.R., 2002. Vapour undersaturation in primitive mid oceanic ridge basalt and the volatile content of Earth's upper mantle. *Nature* 419, 451-455.
- Saccani, E. 2015. A new method of discriminating different types of post-Archean ophiolitic basalts and their tectonic significance using Th-Nb and Ce-Dy-Yb systematics. *Geoscience Frontiers* 6, 481-501.
- Saha, A., Dhang, A., Ray, J., Chakraborty, S., Moecher, D., 2010. Complete preservation of ophiolite suite from south Andaman, India: A mineral-chemical perspective. *Journal of Earth System Science* 119, 365-381
- Saha, A., Manikyamba, C., Santosh, M., Ganguly, S., Khelen, A.C., Subramanyam, K.S.V., 2015. Platinum Group Elements (PGE) geochemistry of komatiites and boninites from Dharwar Craton, India: Implications for mantle melting processes. *Journal of Asian Earth Sciences* 105, 300-319.
- Said, N., Kerrich, R., Maier, W.D., McCuaig, C., 2011. Behaviour of Ni–PGE–Au–Cu in mafic–ultramafic volcanic suites of the 2.7 Ga Kambalda Sequence, Kalgoorlie Terrane, Yilgarn Craton. *Geochimica et Cosmochimica Acta* 75, 2882-2910.

- Santosh, M., Yang, Q.Y., Shaji, E., Tsunogae, T., Ram Mohan, M., Satyanarayanan, M. 2015. An exotic Mesoproterozoic microcontinent: The Coorg Block, southern India. *Gondwana Research* 27, 165-195.
- Santosh, M., Shaji, E., Tsunogae, T., Mohan, M.R., Satyanarayanan, M., Horie, K., 2013. Suprasubduction zone ophiolite from Agali hill: Petrology, zircon SHRIMP U-Pb geochronology, geochemistry and implications for Neoproterozoic plate tectonics in southern India. *Precambrian Research* 231, 301-324.
- Santosh, M., Hari, K.R., He, X.F., Han, Y.S., Manu Prasanth, M.P., 2018. Oldest lamproites from Peninsular India track the onset of Paleoproterozoic plume-induced rifting and the birth of Large Igneous Province. *Gondwana Research* 55, 1-20.
- Saunders, A. D., Tarney, J., Marsh, N. G., Wood, D. A., 1980. Ophiolites as ocean crust or marginal basin crust: a geochemical approach. In *Ophiolites. Proc. Internat. Ophiolite Symp. Geol. Surv. Dept. Cyprus Nicosia*, pp. 193-204.
- Savov, I. P., Ryan, J. G., D'Antonio, M., Kelley, K., Mattie, P., 2005. Geochemistry of serpentinized peridotites from the Mariana Forearc Conical Seamount, ODP Leg 125: Implications for the elemental recycling at subduction zones. *Geochemistry, Geophysics, Geosystems*, 6(4)
- Savov, I. P., Ryan, J. G., D'Antonio, M., Fryer, P., 2007. Shallow slab fluid release across and along the Mariana arc-basin system: Insights from geochemistry of serpentinized peridotites from the Mariana fore arc. *Journal of Geophysical Research: Solid Earth*, 112(B9).
- Sengupta, S., Ray, K. K., Acharyya, S. K., De Smeth, J. B., 1990. Nature of ophiolite occurrences along the eastern margin of the Indian plate and their tectonic significance. *Geology* 18, 439-442.
- Sharma, M., Wasserburg, G. J., 1996. The neodymium isotopic compositions and rare earth patterns in highly depleted ultramafic rocks. *Geochimica et Cosmochimica Acta* 60, 4537-4550.
- Shastri, A., Srivastava, R. K., Chandra, R., Jenner, G. A. 2001. Fe-Ti enriched mafic rocks from south Andaman ophiolite suite: Implication of late stage liquid immiscibility. *Current Science* 80, 453-454.
- Shastri, A., Srivastava, R. K., Chandra, R., Jenner, G. A. 2002. Geochemical characteristics and genesis of oceanic plagiogranites associated with south Andaman ophiolite suite, India: A late stage silicate liquid immiscibility product. *J. Geol. Soc. India* 59, 233-241.
- Shellnutt, J.G., 2014. The Emeishan large igneous province: A synthesis. *Geoscience Frontiers* 5, 369-394.
- Shervais, J. W. 2001. Birth, death, and resurrection: The life cycle of suprasubduction zone ophiolites. *Geochemistry, Geophysics, Geosystems*, 2
- Shervais, J.W., 1982. Ti-V plots and the petrogenesis of modern and ophiolitic lavas: *Earth and Planetary Science Letters* 59, 101-118.
- Shirey, S. B., Walker, R. J. 1998. The Re-Os isotope system in cosmochemistry and high-temperature geochemistry. *Annual Review of Earth and Planetary Sciences* 26, 423-500.

- Singh, M. R., Manikyamba, C., Ray, J., Ganguly, S., Santosh, M., Saha, A., Rambabu, S., Sawant, S. S., 2016. Major, trace and platinum group element (PGE) geochemistry of Archean Iron Ore Group and Proterozoic Malangtoli metavolcanic rocks of Singhbhum Craton, Eastern India: Inferences on mantle melting and sulphur saturation history. *Ore Geology Reviews* 72, 1263-1289.
- Singh, A. K., 2013. Petrology and geochemistry of Abyssal Peridotites from the Manipur Ophiolite Complex, Indo-Myanmar Orogenic Belt, Northeast India: Implication for melt generation in mid-oceanic ridge environment. *Journal of Asian Earth Sciences* 66, 258-276.
- Singh, A. K., Devi, L. D., Singh, N. I., Subramanyam, K. S. V., Singh, R. B., Satyanarayanan, M., 2013. Platinum-group elements and gold distributions in peridotites and associated podiform chromitites of the Manipur Ophiolitic Complex, Indo-Myanmar Orogenic Belt, Northeast India. *Chemie der Erde-Geochemistry* 73, 147-161.
- Sobolev, A. V., Danyushevsky, L. V., 1994. Petrology and geochemistry of boninites from the north termination of the Tonga Trench: constraints on the generation conditions of primary high-Ca boninite magmas. *Journal of Petrology* 35, 1183-1211.
- Song, X. Y., Keays, R. R., Zhou, M. F., Qi, L., Ihlenfeld, C., Xiao, J. F., 2009. Siderophile and chalcophile elemental constraints on the origin of the Jinchuan Ni-Cu-(PGE) sulfide deposit, NW China. *Geochimica et Cosmochimica Acta* 73, 404-424.
- Spandler, C., Pirard, C., 2013. Element recycling from subducting slabs to arc crust: A review. *Lithos* 170, 208-223.
- Stern, R. J., 2002. Crustal evolution in the East African Orogen: a neodymium isotopic perspective. *Journal of African Earth Sciences* 34, 109-117.
- Stern, R. J., 2004. Subduction initiation: spontaneous and induced. *Earth and Planetary Science Letters* 226, 275-292.
- Stern, R.J., Lin, P-N., Morris, J.D., Jackson, M.C., Fryer, P., Bloomer, S.H., Ito, E., 1990. Enriched back-arc basin basalts from the northern Mariana Trough: implications for the magmatic evolution of back-arc basins. *Earth and Planetary Science Letters* 100, 210-225.
- Stern, R.J., Reagan, M., Ishizuka, O., Ohara, Y. and Whattam, S., 2012. To Understand Subduction Initiation, Study Forearc Crust; To Understand Forearc Crust, Study Ophiolites. *Lithosphere* 4, 469-483.
- Straub, S. M., Zellmer, G. F., 2012. Volcanic arcs as archives of plate tectonic change. *Gondwana Research* 21, 495-516.
- Sun, S.S., Mc Donough, W.F., 1989. Chemical and isotopic systematics of oceanic basalts, implications for mantle composition and processes. In: A.D. Saunders, M.J. Norry (Eds.), *Magmatism in the Ocean Basins*. Geological Society of London Special Publication 42, Blackwell Scientific Publication, UK, pp. 313-345.
- Tatsumi, Y., 2005. The subduction factory: how it operates in the evolving Earth. *GSA today* 15, 4.
- Taylor, S. R., McLennan, S. M., 1985. *The continental crust: its composition and evolution*, Oxford, Blackwell, 312 p.

- Ulmer, P., Trommsdorff, V., 1995. Serpentine stability to mantle depths and subduction-related magmatism. *Science* 268, 858-861.
- Ulrich, M., Picard, C., Guillot, S., Chauvel, C., Cluzel, D., Meffre, S. 2010. Multiple melting stages and refertilization as indicators for ridge to subduction formation: The New Caledonia ophiolite. *Lithos* 115, 223-236.
- Umino, S., Kitamura, K., Kanayama, K., Tamura, A., Sakamoto, N., Ishizuka, O., Arai, S., 2015. Thermal and chemical evolution of the subarc mantle revealed by spinel-hosted melt inclusions in boninite from the Ogasawara (Bonin) Archipelago, Japan. *Geology* 43, 151-154.
- Uysal, I., Tarkian, M., Sadiklar, M. B., Şen, C., 2007. Platinum-group-element geochemistry and mineralogy of ophiolitic chromitites from the Kop mountains, Northeastern Turkey. *The Canadian Mineralogist* 45, 355-377.
- Uysal, I., Tarkian, M., Sadiklar, M. B., Zaccarini, F., Meisel, T., Garuti, G., Heidrich, S. 2009. Petrology of Al- and Cr-rich ophiolitic chromitites from the Muğla, SW Turkey: implications from composition of chromite, solid inclusions of platinum-group mineral, silicate, and base-metal mineral, and Os-isotope geochemistry. *Contributions to Mineralogy and Petrology* 158, 659-674.
- van Keken, P. E., Hacker, B. R., Syracuse, E. M., & Abers, G. A., 2011. Subduction factory: 4. Depth-dependent flux of H₂O from subducting slabs worldwide. *Journal of Geophysical Research: Solid Earth* 116(B1).
- Vogel, D.C., Keays, R.R., 1997. The petrogenesis and PGE geochemistry of the Newer Volcanic Province, Victoria, Australia. *Chemical Geology* 136, 181-204.
- Vohra, C. P., Haldar, D., Ghosh Roy, A. K. 1989. The Andaman–Nicobar Ophiolite Complex and associated mineral resources – current appraisal; Phanerozoic Ophiolite of India, Ghose N C (ed.), Sumna Publ., Patna, 281–315
- Volker, D., Wehrmann, H., Kutterolf, S., Iyer, K., Rabbel, W., Geersen, J., Hoernle, K., 2014. Contrasting input and output fluxes of southern-central Chile subduction zone: water, chlorine and sulphur. *International Journal of Earth Science*, <http://dx.doi.org/10.1007/s00531-014-1002-0>.
- Wang, C., Zhao, X., Liu, Z., Lippert, P. C., Graham, S. A., Coe, R. S., ... , Li, Y., 2008. Constraints on the early uplift history of the Tibetan Plateau. *Proceedings of the National Academy of Sciences* 105, 4987-4992.
- Whattam, S. A., Stern, R. J., 2011. The ‘subduction initiation rule’: a key for linking ophiolites, intra-oceanic forearcs, and subduction initiation. *Contributions to Mineralogy and Petrology* 162, 1031-1045.
- Wood, S. A., Mountain, B. W., Pan, P., 1992. The aqueous geochemistry of platinum, palladium and gold; recent experimental constraints and a re-evaluation of theoretical predictions. *The Canadian Mineralogist* 30, 955-982.
- Woodland, S.J., Pearson, D.G., Thirlwall, M.F., 2002. A Platinum Group Element and Re-Os isotope investigation of siderophile element recycling in subduction zones: Comparison of Grenada, Lesser Antilles Arc and Izu-Bonin Arc. *Journal of Petrology* 43, 171-198.

- Xia, B., Yu, H. X., Chen, G. W., Qi, L., Zhao, T. P., Zhou, M. F., 2003. Geochemistry and tectonic environment of the Dagzhuka ophiolite in the Yarlung-Zangbo suture zone, Tibet. *Geochemical Journal* 37, 311-324.
- Xia, X., Song, S., Niu, Yaoling, 2012. Tholeiite–Boninite terrane in the North Qilian suture zone: Implications for subduction initiation and back-arc basin development. *Chemical Geology* 328, 259–277.
- Xiong, F., Yang, J., Robinson, P. T., Gao, J., Chen, Y., Lai, S., 2017. Petrology and geochemistry of peridotites and podiform chromitite in the Xigaze ophiolite, Tibet: Implications for a suprasubduction zone origin. *Journal of Asian Earth Sciences*, 146, 56-75.
- Yang, Q.Y., Santosh, M., 2017. The building of an Archean microcontinent: Evidence from the North China Craton. *Gondwana Research* 50, 3-37.
- Yang, Q.Y., Santosh, M., Ganguly, S., Arun-Gokul, J., Dev, S.D., Tsunogae, T., Shaji, E., Dong, Y. and Manikyamba, C., 2016. Melt-fluid infiltration in Archean suprasubduction zone mantle wedge: Evidence from geochemistry, zircon U-Pb geochronology and Lu-Hf isotopes from Wynad, southern India. *Precambrian Research* 281,101-127.
- Zhao, J. X., Shiraishi, K., Ellis, D. J., Sheraton, J. W., 1995. Geochemical and isotopic studies of syenites from the Yamato Mountains, East Antarctica: implications for the origin of syenitic magmas. *Geochimica et Cosmochimica Acta* 59, 1363-1382.
- Zhao, J.J., Zhou, M.F., 2007. Geochemistry of Neoproterozoic mafic intrusions in the Panzhihua district (Sichuan Province, SW china): implications for subduction related metasomatism in the upper mantle. *Precambrian Research* 152, 27-47.
- Zhou, M. F., Robinson, P. T., Leshner, C. M., Keays, R. R., Zhang, C. J., Malpas, J. 2005. Geochemistry, petrogenesis and metallogenesis of the Panzhihua gabbroic layered intrusion and associated Fe–Ti–V oxide deposits, Sichuan Province, SW China. *Journal of Petrology*, 2253-2280

Figure Caption:

Figure 1. Location of the Tethyan ophiolite belt in the geological map of Indo-Burma-Sumatra subduction zone. Plate boundaries, faults and rates are modified after NASA/Goddard Space Flight Centre, Digital Tectonic Activity, Map of the Earth, 2000; Plates project, University of Texas at Austin; Hall, 2002)

Figure 2. (A) Geological map of the south Andaman (modified after Ray et al., 1988). (B) Geological map of the studied area (modified after Saha et al., 2010). (C) Geological map of the Badmash pahar area.

Figure 3. (A) Field photograph showing occurrence of serpentinized mantle peridotite near Badmash pahar area. (B) Photomicrographs showing typical mesh texture in serpentinized mantle peridotite from the study area. (C) Photomicrographs showing occurrence of opaque minerals (magnetite) along the weak plane of olivine grains and secondary veins.

Figure 4. (A) Al_2O_3 -CaO-MgO plots for mantle peridotites from the study area. Field of mantle peridotite is after Coleman (1977). Data from hartzburgite from Izu-Bonin-Mariana forearc have also been plotted (Data source: Parkinson and Pearce, 1998). (B) Ti vs. V diagram illustrating the studied samples in distinct fields of boninite (after Shervias, 1982). Data from hartzburgite and dunite from Izu-Bonin-Mariana forearc have also been plotted (Data source: Parkinson and Pearce, 1998)

Figure 5. Chondrite normalized REE patterns and primitive mantle normalized trace element patterns for studied mantle peridotite. Normalizing factors are from Sun and McDonough (1989).

Figure 6. Chondrite normalized platinum group element patterns for mantle peridotite (after Dai et al., 2011). Normalizing factors are from McDonough and Sun (1995). The fields of Northwest Anatolian peridotites are from Aldanmaz and Koprubasi (2006); the fields of Luqu peridotites, Xigaze ophiolites from Chen and Xia (2008); both of them represent subduction zone peridotites; the fields of Sumail peridotites, Oman ophiolite from Lorand et al., 2009.

Figure 7. (A) and (B) $(\text{Th})_N$ vs. $(\text{Nb})_N$ diagrams (after Saccani, 2015) showing the tectonic affinity for the studied mantle peridotite samples. (C) Chondrite normalized REE patterns for studied mantle peridotite. Compositional field for the south Sandwich forearc peridotites from Pearce et al. (2000) and field for Dazhuka and Bainang peridotites is from Dubois-Côté et al. (2005). Boninite field is adopted from Hickey and Frey (1982).

Figure 8. (A) CaO vs. Al_2O_3 variation plot (Pearce et al., 1992, Ishii et al., 1992) for studied mantle peridotite. (B) Plot of weight ratios of Mg/Si vs. Al/Si for mantle peridotites, in comparison with fields of peridotites of different origins. The diagram was based on the compositional variation of mantle peridotites compiled by Pearson et al. (2003) and Palme and O'Neill (2003), and abyssal peridotites by Niu (2004). The expected compositional change of residual mantle peridotites during partial melting is shown with a thick gray arrow originating from the primitive mantle values (McDonough and Sun, 1995). Mariana forearc peridotites are from Ishii et al. (1992). (C) Al_2O_3 contents of the whole-rock of the studied mantle peridotite compared with those from other tectonic settings (Azer and Khalil, 2005; Abdel Al et al., 2016).

Figure 9. (A) Chondrite normalized REE patterns mantle peridotites from south Andaman ophiolite suite. The shaded area is also shown for comparison and is the range of model residual mantle compositions (based on Aldanmaz and Korrubasi, 2006). (B) Tb/Yb vs. Al_2O_3 plots for mantle peridotite from south Andaman ophiolite suite. The trends for spinel and garnet melting are from Bodinier et al. (1988) and McDonough and Frey (1989). (C) Ni vs. Ca# plot of compositions of mantle peridotite from south Andaman ophiolite suite. Field of refractory and impregnated abyssal peridotite is also shown (Bodinier and Godard, 2003). (D) Chondrite-normalized $(La/Sm)_N$ vs. $(1/Sm)_N$ diagram (Sharma and Wasserburg, 1996) showing plots of mantle peridotites from south Andaman ophiolite. MORB: Mid-ocean ridge basalts; UM: Upper mantle composition; CC: Continental crust composition; UDM: Ultra-depleted melt composition; HZ1, HZ2 and HZ3: Model harzburgite compositions.

Figure 10. (A) Pd/Ir vs. Ni/Cu diagram showing the plots of mantle peridotite occupying the fields of mantle. Fields are after Barnes, 1990. (B) Pt/Pt* vs. Pd/Ir plots for the studied mantle peridotite. Fractionation and partial melting trends are from Garuti et al., 1997. Fields for mantle peridotite and alpine type peridotite (Garuti et al., 1997) and peridotites from Manipur ophiolite belt (Singh, 2013) are also shown. (C) Chondrite-normalized PPGE/IPGE vs. $\sum PGE$ plot for south Andaman mantle peridotites. Upper mantle values and ophiolitic trend are from Leblanc (1991) and Melcher et al. (1999) respectively. For comparison, fields for podiform chromitites and peridotites from the Manipur Ophiolite Complex (Singh et al., 2013; Singh, 2013); main ore field chromitites, Kempirsai ophiolite massif, Urals (Melcher et al., 1999), podiform chromitites, Eskisehir ophiolite NW-Turkey (Uysalet al., 2009) are shown.

Figure 11. (A) Ni/Pd vs. Cu/Ir plot (after Barnes et al., 1985) showing olivine, chromite and sulphide fractionation trends. The studied samples exhibit olivine and sulphide fractionation trend. (B) Cu vs. Pd (after Hoatson and Keays, 1989) plot showing sulphur undersaturated nature of studied mantle peridotite. (C) Nb/Zr vs. Th/Zr plot showing the studied in an array consistent with fluid-related enrichment of mantle through subduction process (after Zhao and Zhou, 2006).

Figure 12. Cartoon showing schematic model of subduction initiation and fore arc extension in the genesis of mantle peridotite with boninitic lineage in south Andaman ophiolite suite.

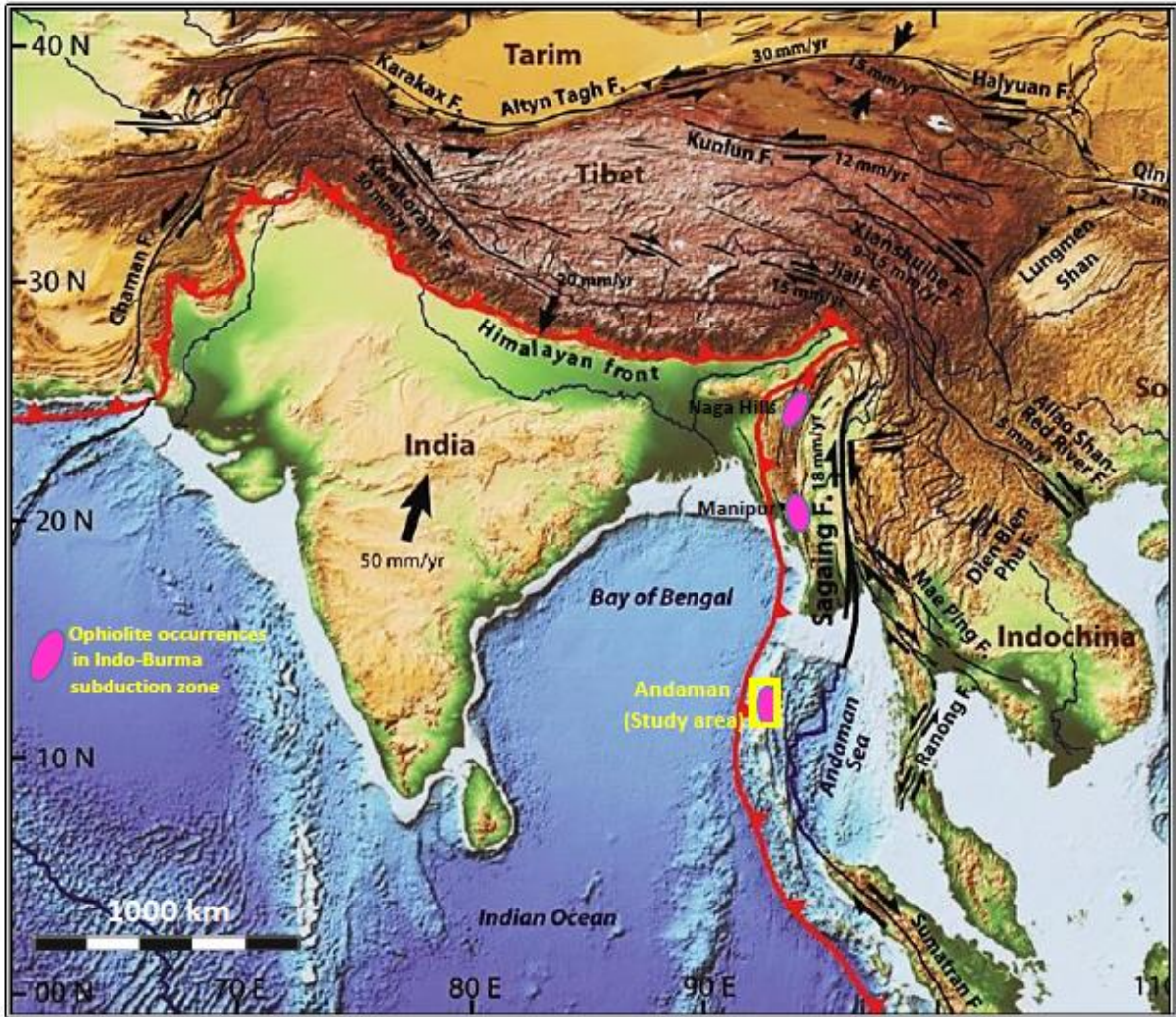


Fig.1

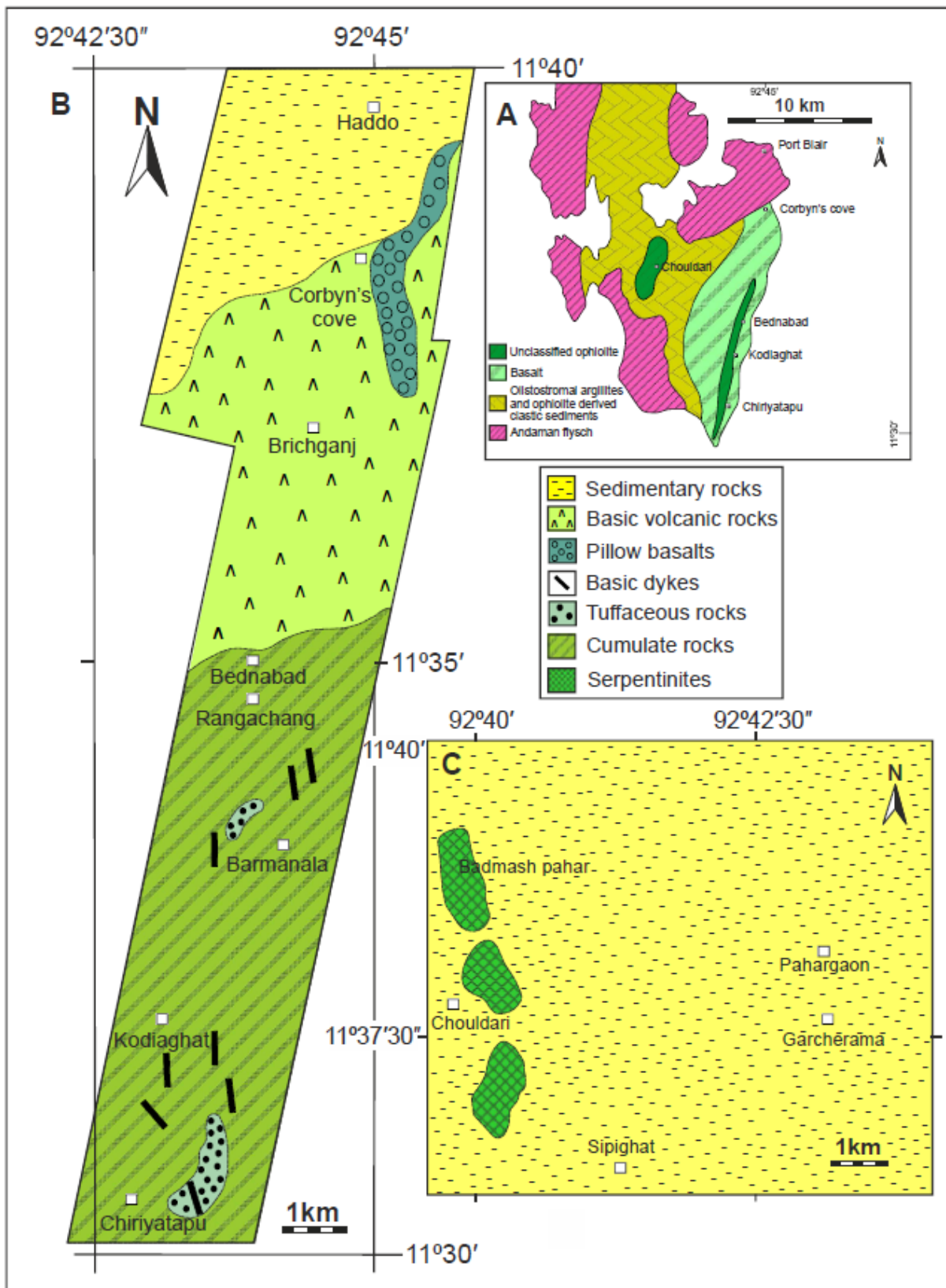


Fig. 2

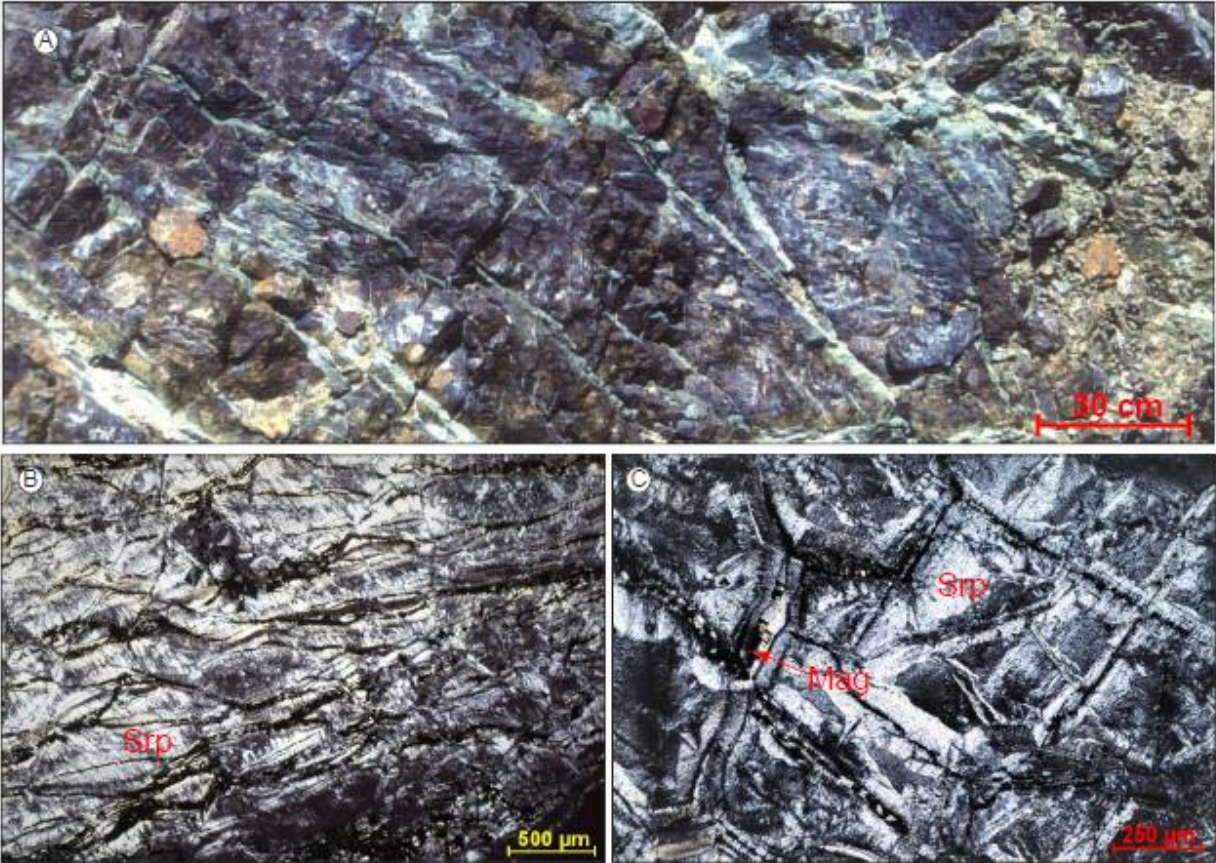


Fig. 3

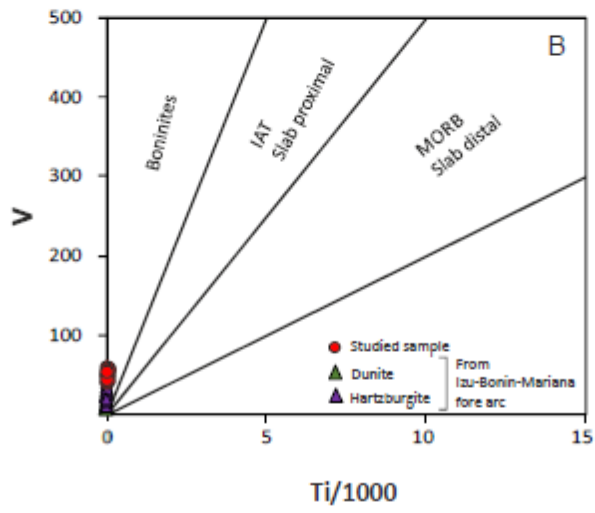
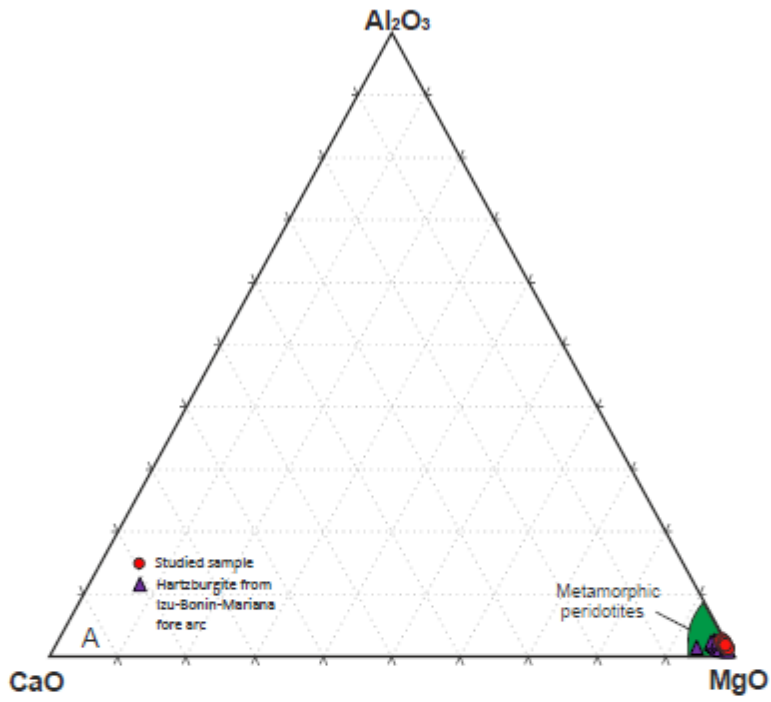


Fig. 4

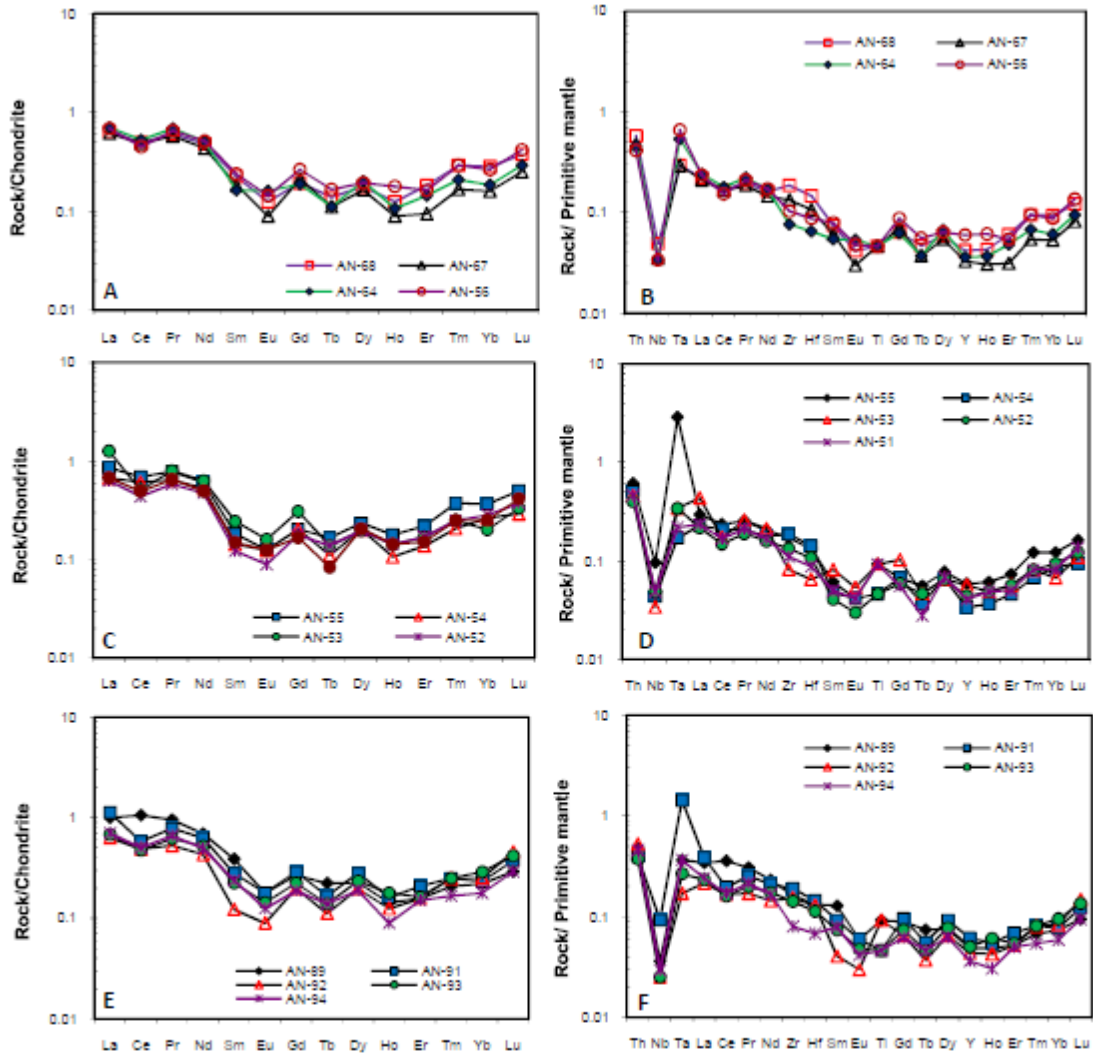


Fig. 5

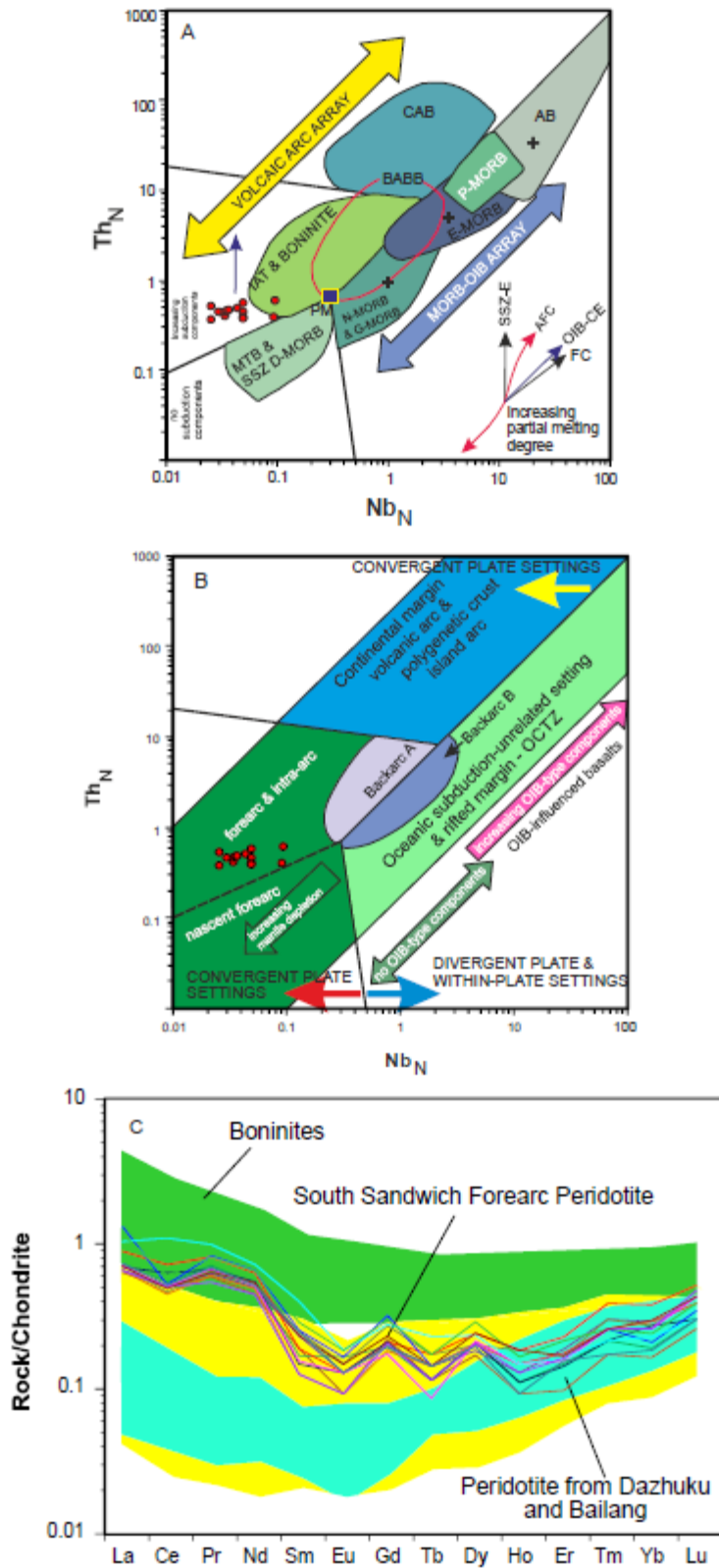


Fig. 7

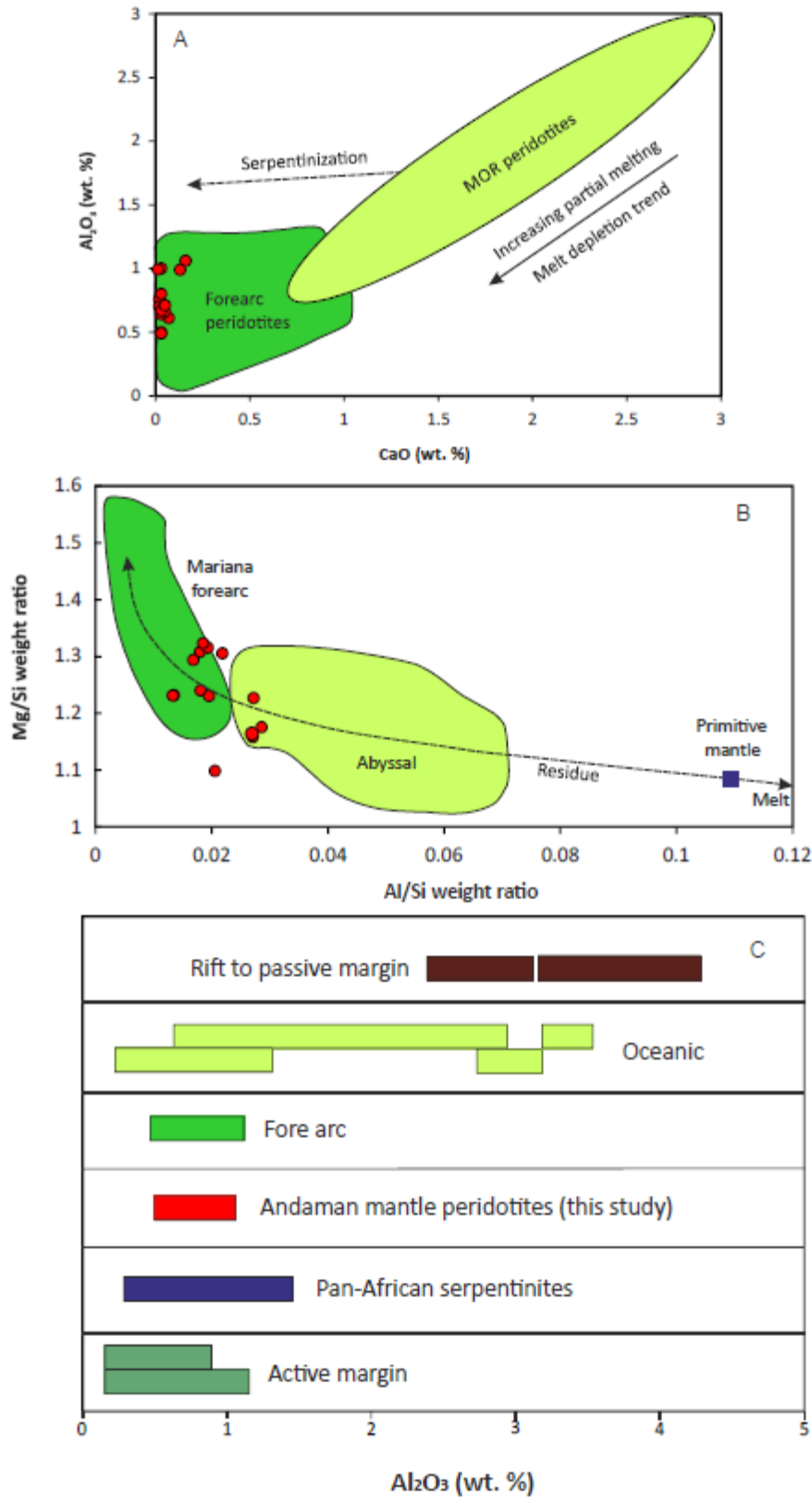


Fig. 8

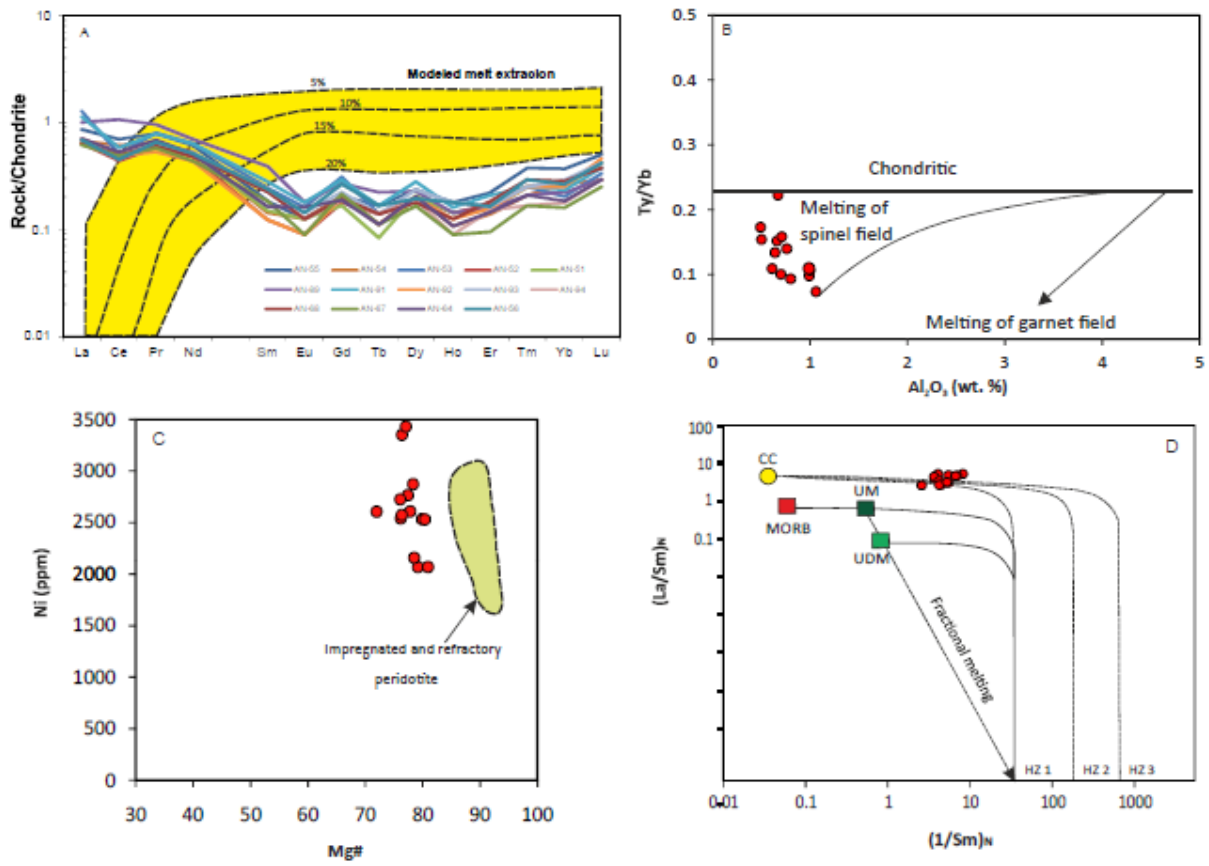


Fig. 9

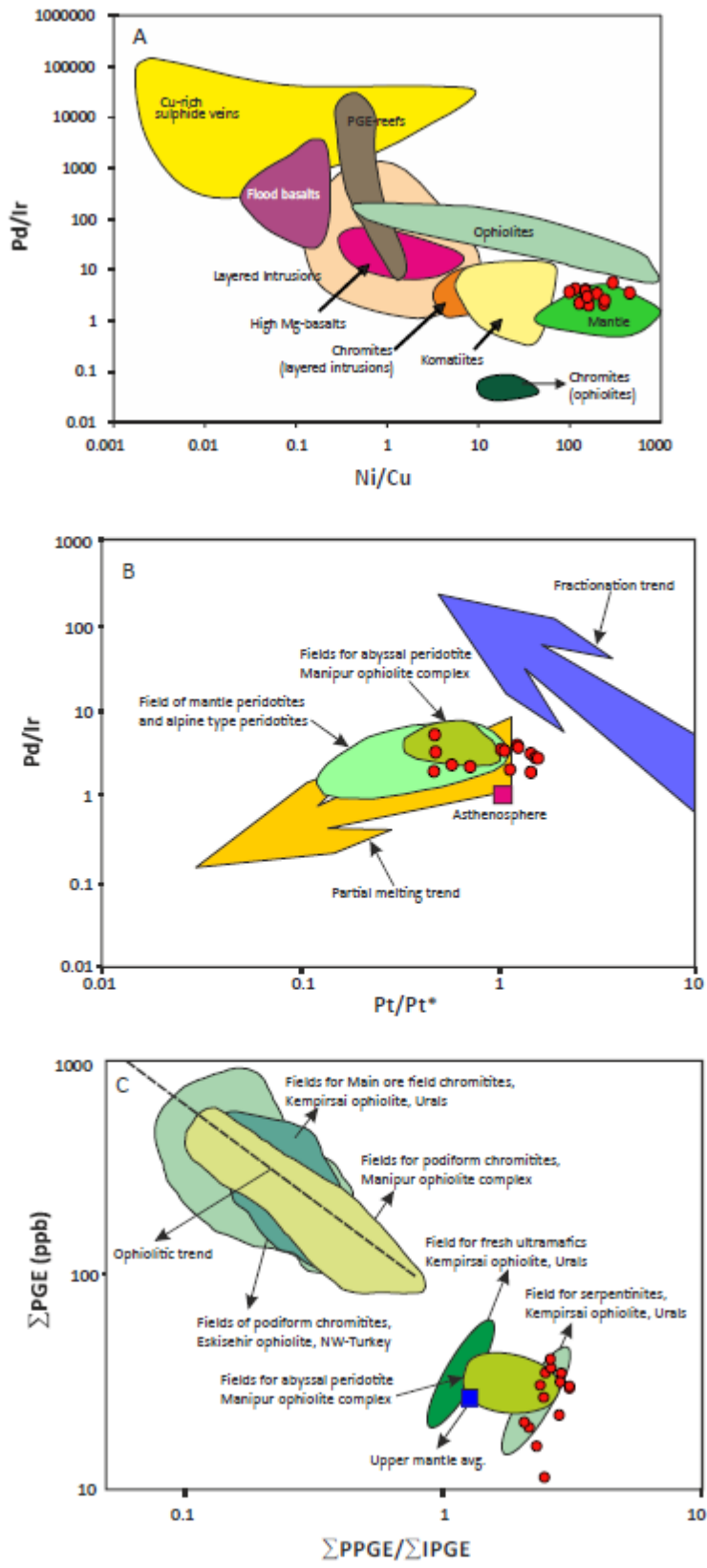


Fig. 10

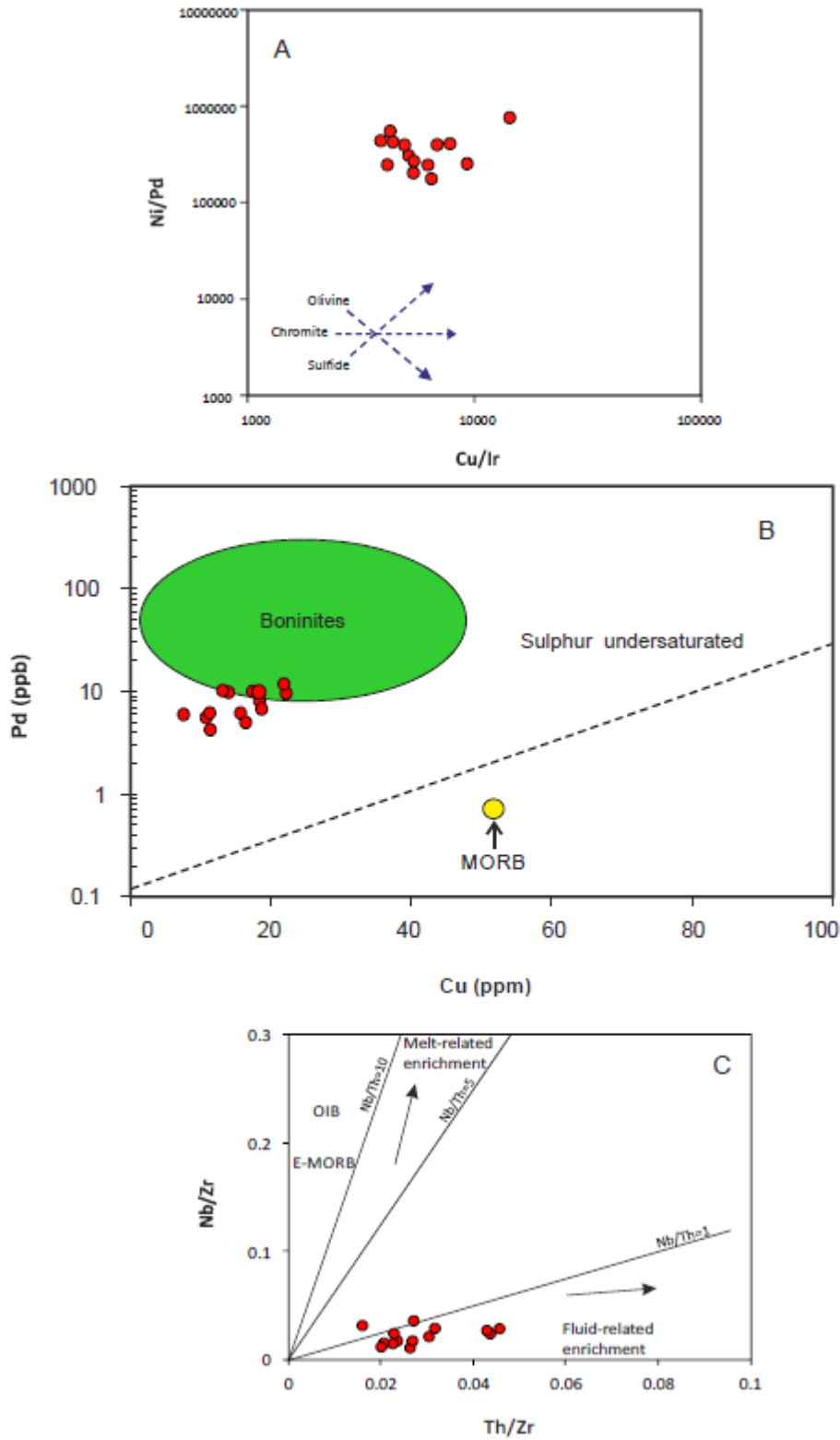


Fig. 11

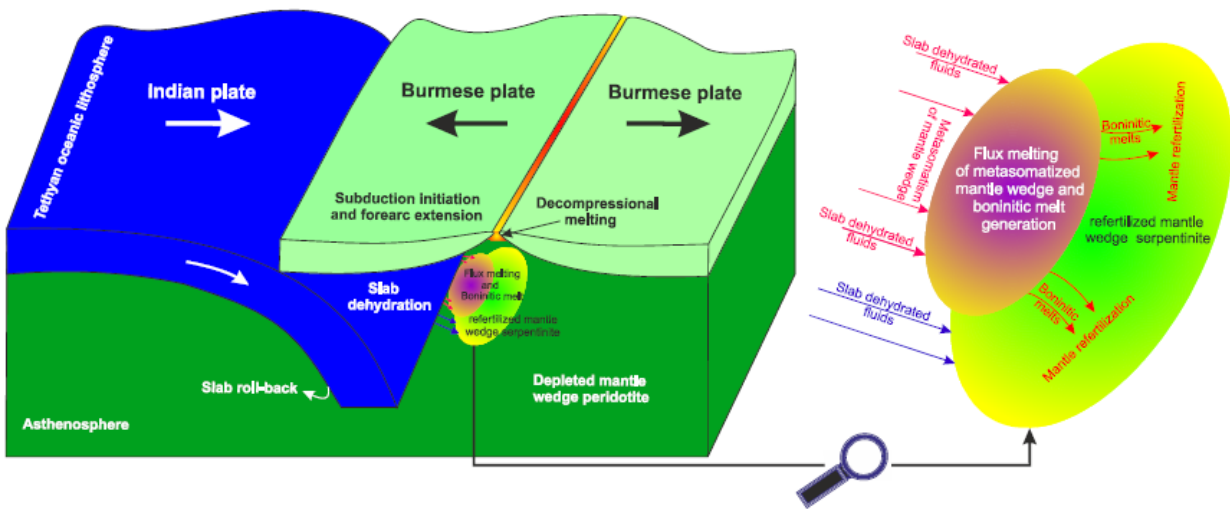


Fig. 12

Table 1. Major, trace, REE and PGE compositions of mantle peridotite from south Andaman ophiolite suite

wt.%	AN-68	AN-67	AN-64	AN-56	AN-55	AN-54	AN-53
SiO ₂	41.13	42.00	40.39	41.91	41.09	41.57	41.36
TiO ₂	0.01	0.01	0.01	0.01	0.02	0.01	0.02
Al ₂ O ₃	0.61	0.50	0.64	0.76	0.70	0.80	0.66
Fe ₂ O ₃	9.06	10.91	8.43	12.09	8.89	10.42	10.68
MnO	0.14	0.12	0.10	0.16	0.13	0.11	0.15
MgO	41.39	40.24	41.10	35.82	42.04	42.21	39.89
CaO	0.07	0.03	0.03	0.02	0.02	0.03	0.05
Na ₂ O	0.01	0.01	0.02	0.02	0.02	0.08	0.01
K ₂ O	0.01	0.01	0.01	0.01	0.01	0.03	0.01
P ₂ O ₅	0.20	0.20	0.20	0.20	0.20	0.20	0.02
LOI	6.87	5.31	8.61	9.07	6.59	4.24	7.21
Total	99.50	99.34	99.54	100.07	99.71	99.70	100.06
Mg#	80	76	81	72	80	78	76
<i>ppm</i>							
Cr	2700	1068	1917	2783	2972	2889	2459
Co	123	106	92	119	112	107	98
Ni	2533	2539	2071	2605	2530	2609	3350
Rb	0.48	0.42	0.45	0.51	0.50	0.55	0.60
Sr	6.58	3.63	2.81	4.87	2.95	3.26	5.85
Cs	0.03	0.02	0.02	0.03	0.02	0.03	0.02
Ba	13.00	7.34	7.78	18.55	7.22	7.39	11.32
Sc	11.08	6.66	8.57	10.90	11.59	10.94	9.25
V	57.16	34.82	37.01	44.74	51.93	46.08	44.93
Ta	0.01	0.01	0.02	0.03	0.12	0.01	0.01
Nb	0.04	0.03	0.02	0.02	0.07	0.03	0.02
Zr	2.09	1.49	0.86	1.15	1.92	2.08	0.91
Hf	0.05	0.03	0.02	0.03	0.04	0.04	0.02
Th	0.05	0.04	0.04	0.04	0.05	0.04	0.04
U	0.01	0.01	0.00	0.01	0.00	0.01	0.01
Y	0.19	0.15	0.16	0.27	0.27	0.15	0.26
La	0.15	0.14	0.17	0.16	0.20	0.16	0.30
Ce	0.30	0.29	0.32	0.27	0.42	0.37	0.31
Pr	0.05	0.05	0.06	0.06	0.07	0.06	0.07
Nd	0.22	0.20	0.23	0.23	0.28	0.24	0.29
Sm	0.03	0.03	0.02	0.04	0.03	0.02	0.04
Eu	0.01	0.01	0.01	0.01	0.01	0.01	0.01
Gd	0.04	0.04	0.04	0.05	0.04	0.04	0.06
Tb	0.01	0.00	0.00	0.01	0.01	0.00	0.01
Dy	0.04	0.04	0.05	0.05	0.06	0.05	0.05
Ho	0.01	0.01	0.01	0.01	0.01	0.01	0.01
Er	0.03	0.02	0.02	0.03	0.04	0.02	0.03
Tm	0.01	0.00	0.01	0.01	0.01	0.01	0.01
Yb	0.05	0.03	0.03	0.04	0.06	0.04	0.03
Lu	0.01	0.01	0.01	0.01	0.01	0.01	0.01
ΣREE	0.94	0.86	0.97	0.97	1.23	1.03	1.20
Cu	22.26	10.85	14.01	18.43	15.76	13.21	11.44
Zn	45.44	44.93	43.14	33.28	37.57	37.73	50.96
Ga	1.26	0.68	0.78	1.12	1.02	0.92	1.00
Pb	15.86	12.04	16.26	11.25	15.71	12.83	12.04

Table 1. Cond...

<i>ppb</i>	AN-68	AN-67	AN-64	AN-56	AN-55	AN-54	AN-53
Ru	5.20	4.40	5.20	8.00	5.60	6.20	2.80
Rh	0.60	1.00	0.60	2.40	0.60	0.60	0.40
Pd	10.00	5.80	10.20	8.40	6.40	10.60	4.40
Os	2.40	2.20	2.40	3.00	2.60	3.20	1.20
Ir	2.40	2.80	2.60	3.60	3.20	3.20	0.80
Pt	9.60	3.60	9.80	10.20	9.00	11.60	2.00
ΣPGE	30.2	19.8	30.8	35.6	27.4	35.4	11.6
ΣIPGE	10.0	9.4	10.2	14.6	11.4	12.6	4.8
ΣPPGE	20.2	10.4	20.6	21.0	16.0	22.8	6.8
Al ₂ O ₃ /TiO ₂	61	50	64	76	35	80	33
CaO/Al ₂ O ₃	0.11	0.06	0.05	0.03	0.03	0.04	0.08
(La/Sm) _N	2.84	3.34	4.30	2.88	4.68	4.68	5.18
(Ce/Yb) _N	1.75	3.05	2.87	1.70	1.89	2.31	2.51
(Gd/Yb) _N	0.68	1.34	1.02	1.00	0.55	0.77	1.53
ΣPPGE/ΣIPGE	3.02	2.11	3.02	2.44	2.40	2.81	2.42
ΣIPGE/ΣPPGE	0.50	0.90	0.50	0.70	0.71	0.55	0.71
Pt/Pt*	1.27	0.48	1.28	0.74	1.49	1.49	0.49
Ni/Cu	114	234	148	141	161	198	293
Ni/Pd	253266	437828	203053	310158	395359	246144	761405
Cu/Pd	2226	1870	1374	2194	2462	1246	2601
Cu/Pt	2319	3013	1430	1807	1751	1138	5722
Cu/Ir	9275	3874	5390	5119	4924	4127	14304
Pd/Ir	4.17	2.07	3.92	2.33	2.00	3.31	5.50
Pd/Pt	1.04	1.61	1.04	0.82	0.71	0.91	2.20
Pt/Pd	0.96	0.62	0.96	1.21	1.41	1.09	0.45

Normalization factor after Sun and McDonough(1989)

Table 1. Cond...

wt.%	AN-52	AN-51	AN-89	AN-91	AN-92	AN-93	AN-94
SiO ₂	41.66	42.06	41.05	41.25	41.49	41.69	41.84
TiO ₂	0.01	0.02	0.02	0.01	0.02	0.01	0.01
Al ₂ O ₃	0.99	1.06	0.67	0.71	0.99	1.00	0.49
Fe ₂ O ₃	9.52	10.32	9.62	10.17	8.96	9.45	10.91
MnO	0.16	0.16	0.11	0.14	0.15	0.10	0.12
MgO	37.71	38.45	42.24	39.47	37.37	39.78	40.07
CaO	0.01	0.16	0.03	0.05	0.13	0.03	0.03
Na ₂ O	0.01	0.01	0.02	0.02	0.01	0.01	0.01
K ₂ O	0.01	0.01	0.01	0.01	0.01	0.01	0.01
P ₂ O ₅	0.20	0.20	0.20	0.20	0.20	0.20	0.20
LOI	9.34	7.36	5.79	7.46	9.84	6.98	5.89
Total	99.62	99.81	99.76	99.49	99.17	99.26	99.58
Mg#	77	76	79	77	78	78	76
<i>ppm</i>							
Cr	2633	2951	2042	2421	2921	2625	1453
Co	121	115	93	100	127	91	115
Ni	2766	2573	2068	3432	2872	2158	2724
Rb	0.49	0.49	0.64	0.49	0.42	0.46	0.49
Sr	2.25	2.25	3.29	4.09	3.25	2.63	2.81
Cs	0.02	0.02	0.03	0.02	0.02	0.02	0.02
Ba	7.30	7.71	7.43	9.05	7.16	7.80	9.05
Sc	10.76	10.72	8.48	9.75	11.05	10.85	8.08
V	50.52	55.80	38.08	45.34	52.80	51.89	39.82
Ta	0.01	0.01	0.02	0.06	0.01	0.01	0.02
Nb	0.04	0.04	0.03	0.07	0.02	0.02	0.02
Zr	1.49	1.23	1.82	2.13	1.71	1.60	0.90
Hf	0.03	0.03	0.04	0.05	0.04	0.04	0.02
Th	0.03	0.04	0.04	0.03	0.05	0.03	0.04
U	0.00	0.00	0.00	0.00	0.00	0.00	0.00
Y	0.20	0.19	0.22	0.28	0.20	0.23	0.17
La	0.15	0.16	0.24	0.27	0.15	0.16	0.17
Ce	0.26	0.30	0.64	0.35	0.30	0.29	0.30
Pr	0.05	0.06	0.09	0.07	0.05	0.06	0.06
Nd	0.21	0.22	0.31	0.29	0.20	0.24	0.23
Sm	0.02	0.02	0.06	0.04	0.02	0.03	0.04
Eu	0.01	0.01	0.01	0.01	0.01	0.01	0.01
Gd	0.04	0.03	0.05	0.06	0.04	0.04	0.04
Tb	0.01	0.00	0.01	0.01	0.00	0.01	0.01
Dy	0.05	0.05	0.06	0.07	0.05	0.06	0.05
Ho	0.01	0.01	0.01	0.01	0.01	0.01	0.01
Er	0.03	0.02	0.03	0.03	0.03	0.03	0.02
Tm	0.01	0.01	0.01	0.01	0.01	0.01	0.00
Yb	0.05	0.04	0.04	0.04	0.04	0.05	0.03
Lu	0.01	0.01	0.01	0.01	0.01	0.01	0.01
ΣREE	0.89	0.94	1.54	1.25	0.89	0.98	0.95
Cu	18.37	17.48	16.48	7.65	18.74	21.95	11.35
Zn	39.75	37.40	97.63	38.37	38.61	41.68	40.83
Ga	1.12	1.08	0.93	1.02	1.17	0.95	0.84
Pb	15.84	16.65	17.41	10.57	11.51	16.38	19.98

Table 1. Cond...

<i>ppb</i>	AN-52	AN-51	AN-89	AN-91	AN-92	AN-93	AN-94
Ru	8.20	6.20	4.20	3.80	8.40	7.60	4.80
Rh	0.60	0.80	1.00	0.40	0.60	1.00	0.60
Pd	10.20	10.40	5.20	6.20	7.00	12.20	6.40
Os	3.00	2.60	1.60	1.60	2.60	5.20	3.00
Ir	3.40	2.80	2.40	1.80	2.40	3.40	2.60
Pt	12.00	9.40	8.20	2.40	10.20	11.80	3.60
Σ PGE	37.4	32.2	22.6	16.2	31.2	41.2	21.0
Σ IPGE	14.6	11.6	8.2	7.2	13.4	16.2	10.4
Σ PPGE	22.8	20.6	14.4	9.0	17.8	25.0	10.6
Al ₂ O ₃ /TiO ₂	99	53	34	71	50	100	49
CaO/Al ₂ O ₃	0.01	0.15	0.04	0.07	0.13	0.03	0.06
(La/Sm) _N	5.18	4.55	2.58	4.04	5.14	3.03	2.97
(Ce/Yb) _N	1.55	1.96	4.80	2.49	1.95	1.65	2.83
(Gd/Yb) _N	0.63	0.67	1.22	1.24	0.79	0.77	1.06
Σ PPGE/ Σ IPGE	2.56	2.78	2.76	2.25	2.33	2.54	2.02
Σ IPGE/ Σ PPGE	0.64	0.56	0.57	0.80	0.75	0.65	0.98
Pt/Pt*	1.57	1.05	1.16	0.49	1.61	1.09	0.59
Ni/Cu	151	147	126	449	153	98	240
Ni/Pd	271156	247379	397724	553578	410222	176915	425674
Cu/Pd	1801	1681	3169	1233	2677	1799	1774
Cu/Pt	1531	1860	2010	3185	1837	1860	3154
Cu/Ir	5403	6243	6866	4247	7808	6455	4367
Pd/Ir	3.00	3.71	2.17	3.44	2.92	3.59	2.46
Pd/Pt	0.85	1.11	0.63	2.58	0.69	1.03	1.78
Pt/Pd	1.18	0.90	1.58	0.39	1.46	0.97	0.56

Normalization factor after Sun and McDonough(1989)

Table S1. Major and trace concentrations of UB-N from XRF and ICP-MS

wt%	UB-N			
	A	B	SD	%RSD
SiO ₂	39.77	39.43	0.24	0.60
Al ₂ O ₃	2.77	2.90	0.09	3.32
Fe ₂ O ₃	8.52	8.34	0.13	1.49
MnO	0.13	0.12	0.01	5.44
MgO	35.31	35.21	0.07	0.20
CaO	1.25	1.20	0.04	2.83
Na ₂ O	0.10	0.10	0.00	0.00
K ₂ O	0.02	0.02	0.00	3.37
TiO ₂	0.11	0.11	0.00	1.26
P ₂ O ₅	0.04	0.04	0.00	1.72
<i>ppm</i>				
Sc	13	13	0.20	1.58
V	74	75	1.03	1.38
Cr	2294	2300	1.72	0.08
Co	99	100	3.09	3.04
Ni	1989	2000	9.66	0.48
Cu	28	28	0.94	3.31
Zn	84	85	3.97	4.53
Ga	3	3	0.10	3.30
Rb	4	4	0.06	1.50
Sr	9	9	0.11	1.20
Y	2.5	2.5	0.03	1.11
Zr	3.98	4	0.07	1.78
Nb	0.05	0.05	0.003	5.936
Cs	10	10	0.08	0.86
Ba	26	27	0.26	0.98
La	0.34	0.35	0.004	1.17
Ce	0.8	0.8	0.01	1.49
Pr	0.12	0.12	0.005	4.140
Nd	0.6	0.6	0.02	2.71
Sm	0.2	0.2	0.01	4.79
Eu	0.08	0.08	0.002	2.936
Gd	0.3	0.3	0.01	3.16
Tb	0.06	0.06	0.004	6.477
Dy	0.36	0.38	0.02	5.28
Ho	0.09	0.09	0.005	5.298
Er	0.27	0.28	0.01	3.10
Tm	0.045	0.049	0.004	7.979
Yb	0.27	0.28	0.02	7.94
Lu	0.048	0.045	0.001	2.395
Hf	0.1	0.1	0.005	5.455
Ta	0.02	0.02	0.001	4.809
Pb	13	13	0.30	2.29
Th	0.07	0.07	0.004	5.446
U	0.07	0.07	0.004	5.493

A: present study average of six values; B: reorted values from Govindaraju(1994);GEOREM (georem.mpch-mainz.gwdg.de)

Table S1 Contd... PGE data obtained for standard reference materials of WPR-1 and WMG-1 with

Relative standard Deviation (RSD)

		WPR-1				WMG-1			
		Certified Value*	ICP-MS Obtained Value [†]	Standard Deviation	% RSD	Certified Value*	ICP-MS Obtained Value [†]	Standard Deviation	% RSD
Ru101	ng/g	21.6	21.9	2	9	27.6	34.9	2	5.3
Rh103	ng/g	13.4	13.1	2	7.7	25.6	26.2	1.5	5.6
Pd105	ng/g	235	233.9	9	4.3	307.8	378	18	408
Ir193	ng/g	13.5	13.8	1.5	10.1	44.5	46	2	4.3
Pt195	ng/g	285	284.3	12	5.4	892	871	41	4.7
Au197	ng/g	42.2	41.8	3	7.2	82.4	99	5	4.2

Table S2. Major oxide composition and CIPW norm of mantle peridotites from south Andaman ophiolite suite

	AN-68	AN-67	AN-64	AN-56	AN-55	AN-54	AN-53	AN-52	AN-51	AN-89	AN-91	AN-92	AN-93	AN-94
SiO ₂	41.13	42.00	40.39	41.91	41.09	41.57	41.36	41.66	42.06	41.05	41.25	41.49	41.69	41.84
TiO ₂	0.01	0.01	0.01	0.01	0.02	0.01	0.02	0.01	0.02	0.02	0.01	0.02	0.01	0.01
Al ₂ O ₃	0.61	0.50	0.64	0.76	0.70	0.80	0.66	0.99	1.06	0.67	0.71	0.99	1.00	0.49
Fe ₂ O ₃	9.06	10.91	8.43	12.09	8.89	10.42	10.68	9.52	10.32	9.62	10.17	8.96	9.45	10.91
MnO	0.14	0.12	0.10	0.16	0.13	0.11	0.15	0.16	0.16	0.11	0.14	0.15	0.10	0.12
MgO	41.39	40.24	41.10	35.82	42.04	42.21	39.89	37.71	38.45	42.24	39.47	37.37	39.78	40.07
CaO	0.07	0.03	0.03	0.02	0.02	0.03	0.05	0.01	0.16	0.03	0.05	0.13	0.03	0.03
Na ₂ O	0.01	0.01	0.02	0.02	0.02	0.08	0.01	0.01	0.01	0.02	0.02	0.01	0.01	0.01
K ₂ O	0.01	0.01	0.01	0.01	0.01	0.03	0.01	0.01	0.01	0.01	0.01	0.01	0.01	0.01
P ₂ O ₅	0.20	0.20	0.20	0.20	0.20	0.20	0.02	0.20	0.20	0.20	0.20	0.20	0.20	0.20
LOI	6.87	5.31	8.61	9.07	6.59	4.24	7.21	9.34	7.36	5.79	7.46	9.84	6.98	5.89
Total	99.50	99.34	99.54	100.07	99.71	99.70	100.06	99.62	99.81	99.76	99.49	99.17	99.26	99.58
Plagioclase	0.08	0.08	0.17	0.17	0.17	0.68	0.2	0.2	0.08	0.17	0.17	0.08	0.08	0.08
Orthoclase	0.06	0.06	0.06	0.06	0.06	0.18	0.06	0.06	0.06	0.06	0.06	0.06	0.06	0.06
Corundum	0.58	0.47	0.6	0.72	0.66	0.64	0.59	0.98	1.03	0.63	0.67	0.96	0.97	0.46
Hypersthene	34.02	39.8	32.08	50.31	32.08	31.84	38.36	45.16	44.46	31.45	39.01	45.24	39.91	39.69
Olivine	48.4	42.35	49.26	27.26	50.90	51.36	42.74	34.18	35.96	51.69	41.55	33.52	41.47	42.13
Ilmenite	0.02	0.02	0.02	0.02	0.04	0.02	0.04	0.02	0.04	0.04	0.02	0.04	0.02	0.02
Magnetite	0.43	0.36	0.3	0.49	0.37	0.33	0.43	0.49	0.46	0.3	0.43	0.43	0.3	0.36
Hematite	8.76	10.66	8.22	11.75	8.64	10.19	10.38	9.18	10	9.41	9.87	8.66	9.24	10.66
Apatite	0.46	0.46	0.46	0.46	0.46	0.46	0.05	0.46	0.46	0.46	0.46	0.46	0.46	0.46